FOSSIL

DOE/PC/88651-T1
(DE90006270)

MHD COMPRESSOR–EXPANDER CONVERSION SYSTEM INTEGRATED WITH A GCR INSIDE A DEPLOYABLE REFLECTOR

Project Final Report

REPRODUCED FROM BEST
AVAILABLE COPY

April 20, 1989

Work Performed Under Contract No. AC22-88PC88651

For
U. S. Department of Energy
Pittsburgh Energy Technology Center
Pittsburgh, Pennsylvania

By
ANSALDO S.p.A.
Genova, Italy

DISCLAIMER

This report was prepared as an account of work sponsored by an agency of the United States Government. Neither the United States Government nor any agency Thereof, nor any of their employees, makes any warranty, express or implied, or assumes any legal liability or responsibility for the accuracy, completeness, or usefulness of any information, apparatus, product, or process disclosed, or represents that its use would not infringe privately owned rights. Reference herein to any specific commercial product, process, or service by trade name, trademark, manufacturer, or otherwise does not necessarily constitute or imply its endorsement, recommendation, or favoring by the United States Government or any agency thereof. The views and opinions of authors expressed herein do not necessarily state or reflect those of the United States Government or any agency thereof.

DISCLAIMER

Portions of this document may be illegible in electronic image products. Images are produced from the best available original document.

DOE/PC/88651-T1
(DE90006270)
Distribution Category UC-112

G. Tuninetti*

E. Botta, C. Criscuolo, F. Riscossa**

F. Giammanco°, M. Rosa-Clot°°

DOE/PC/88651--T1

DE90 006270

*Research Division, ANSALDO SpA

**Nuclear Division, ANSALDO SpA

°Department of Physics, University of Pisa

°°Department of Physics, University of Florence

PAGE BLANK

CONTENTS

EXECUTIVE SUMMARY 5

1 INTRODUCTION 8

1.1 Project Objectives 8

1.2 Report Organization 9

Tables and Figures 10

2 PROJECT DESCRIPTION 11

3 REFLECTOR MODELING 13

3.1 Symbols, Terms and Abbreviations 13

3.2 Reference Core Description 15

3.3 Analysis Codes 19

3.4 Features of Performed Calculations 21

3.5 Nuclear Cross Section Calculations 23

3.6 Reactor Calculations 26

3.7 Reactivity Requirements 27

3.8 References 30

Tables and Figures 32

4 WORKING FLUID CHARACTERISTICS 50

4.1 Symbols, Terms and Abbreviations 50

4.2 Phase I 52

4.3 Phase II 54

4.4 Phase III 63

4.5 References 69

5 ELECTRICAL CONDUCTIVITY EFFECTS 70

5.1 Symbols, Terms and Abbreviations 70

5.2 Channel Characteristics and Conductivity 73

5.3 Fission and Gamma Density in the Channel 77

5.4 Conductivity Calculations 81

5.5 References 91

Tables and Figures 93

6 SUMMARY AND CONCLUSIONS 106

7 REPORT DISTRIBUTION LIST 110

EXECUTIVE SUMMARY

CONTRACT TITLE AND NUMBER:

MHD Compressor - Expander Conversion System Integrated with a GCR Inside a Deployable Reflector.

DE-AC22-88PC88651

CONTRACTOR NAME AND ADDRESS:

ANSALDO S.p.A.

Corso F.M. Perrone, 25

16161 Genova - Italy

START DATE: 4-21-1988

COMPLETION DATE: 4-20-1989

This work originates from the proposal "MHD Compressor-Expander Conversion System Integrated with a GCR Inside a Deployable Reflector" submitted by ANSALDO under PRDA RA-22-87PC90271, January 1987. The proposal concerned an innovative concept of nuclear, closed-cycle MHD converter for power generation on space-based systems in the multi-megawatt range. The basic element of this converter is the Power Conversion Unit (PCU) consisting of a gas core reactor directly coupled to an MHD expansion channel. Integrated with the PCU, a deployable reflector provides reactivity control. The working fluid could

be either uranium hexafluoride or a mixture of uranium hexafluoride and helium, added to enhance the heat transfer properties. The original Statement of Work, which concerned the whole conversion system, was subsequently redirected and focused on the basic mechanisms of neutronics, reactivity control, ionization and electrical conductivity in the PCU. Furthermore, the study was required to be "inherently generic such that the analysis and results can be applied to various nuclear reactor and/or MHD channel designs".

Specific goals of the project were:

- To evaluate the performance of the external reflector.
- To determine the influence of additional, fission-induced mechanisms on the ionization levels of the working fluid.
- To estimate the electrical conductivity levels that can be attained in the MHD channel, taking into account the effects of F- or other negative ions.

Two major conclusions can be drawn from the accomplishment of this project:

- A reactor configuration has been obtained which avoids to decouple the neutronics of the cavity and its internal reflector from the external shell, thus enabling the latter to be used for reactivity control.

In particular the results show that the movable reflector is able to make the reactor subcritical by 1000 pcm at least, and to control the reactor from CZP to HFP condition, accounting for a reactivity change up to 3300 pcm associated to depletion.

- The conditions expected in the MHD channel show that the ionization and conductivity levels can be amplified through 'secondary' processes induced by the 'primary' hot electrons which are directly generated by the fission reactions.

The numerical calculations suggest that conductivity levels in the range 10-100 $(\Omega m)^{-1}$ are consistent with the characteristics of short nozzle, high power density generators. In fact, the nozzle length turns out to be of critical importance because of the sharp decrease of residual fission and gamma densities as a function of the distance from the reactor outlet.

This conclusion remains true even if the effect of dissociation and attachment are included in the numerical model.

Furthermore, a preliminary evaluation of the influence of wall material and thickness shows the potential for the fission and gamma densities in the duct to be increased of one order of magnitude, in comparison with the values used in the conductivity calculations, if a material with favourable nuclear properties is adopted.

1 INTRODUCTION

1.1 Project Objectives

This work concerned an innovative concept of nuclear, closed-cycle MHD converter for power generation on space-based systems in the multi-megawatt range. A schematic diagram of the concept is shown in Fig. 1.1. The basic element of this converter is the Power Conversion Unit (PCU) consisting of a gas core reactor directly coupled to an MHD expansion channel. The working fluid could be either uranium hexafluoride or a mixture of uranium hexafluoride and helium, added to enhance the heat transfer properties.

Two major items, both concerning the PCU, were addressed in the project:

1. Because of the high levels of temperature expected in the reactor cavity, reactivity control is not achieved by neutron absorbers (control rods) located in the cavity, but by moving part of the reflector, located outside the pressure vessel, in order to change the amount of neutrons escaping from the core.
2. The mere levels of temperature, however, cannot sustain levels of ionization and, hence, of conductivity, capable of providing efficient power generation in the MHD channel.

   Fission products may represent a possible additional source of ionization.

This report documents the results of work done to investigate these aspects of the proposed concept. ANSALDO addressed both item 1. and 2.: the latter required the scientific support of the Universities of Florence and Pisa, Department of Physics.

1.2 Report Organization

Section 3., Reflector Modeling, illustrates the reactor configuration, as defined throughout contract work, describes the codes and procedures adopted in the analysis, and presents the results concerning the performance of the external movable reflector.

Section 4., Working Fluid Characteristics, investigates the fission-induced ionization mechanisms acting in the working gas, and provides a system of simplified rate equations for numerical solution.

Section 5., Electrical Conductivity Effects, addresses the study of the electrical conductivity levels in the MHD channel, and presents the results of numerical estimates performed with different gas and duct parameters.

References, Tables and Figures are located at the end of each section.

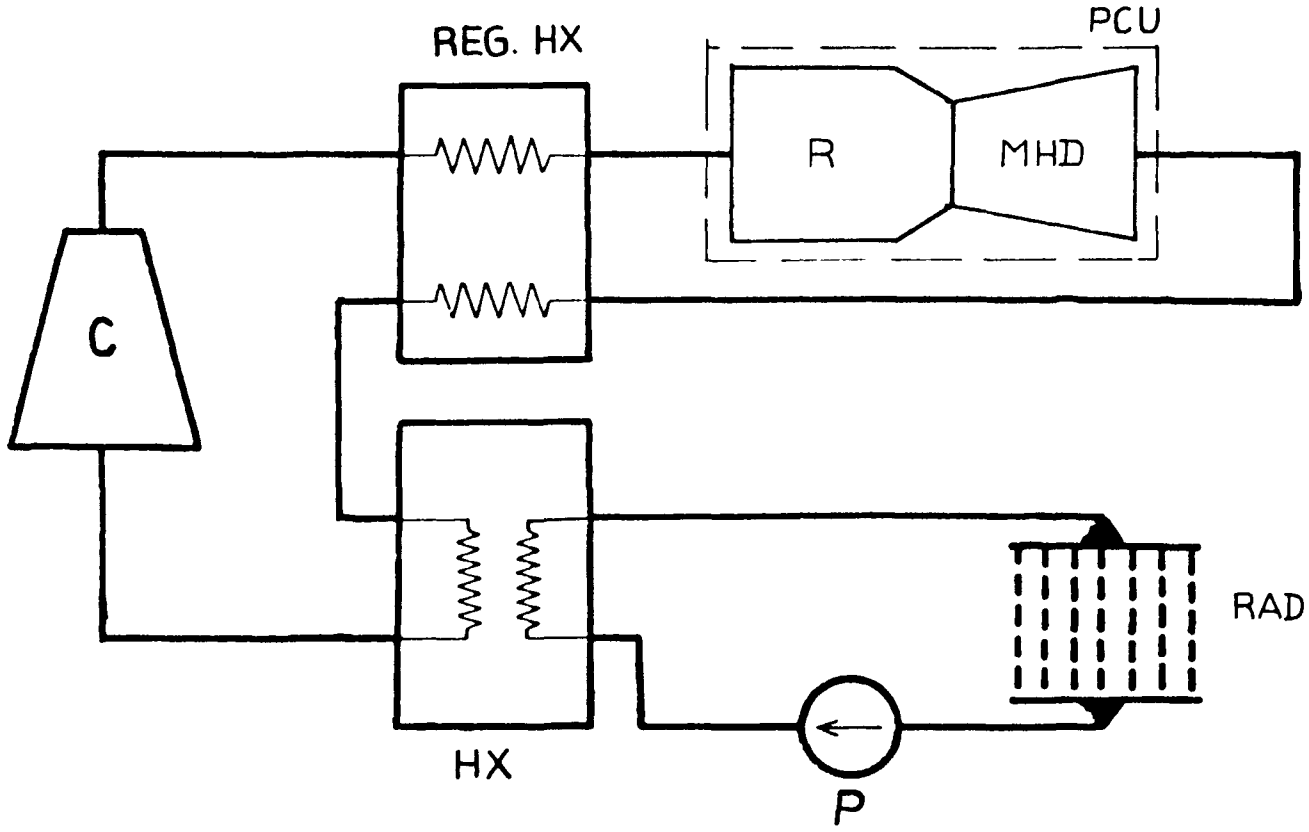

R = REACTOR
MHD = MHD CHANNEL
REG.HX = REGENERATIVE HEAT EXCHANGER
HX = HEAT EXCHANGER

RAD - RADIATOR
P = PUMP
C = COMPRESSOR
PCU - POWER CONVERSION UNIT

Fig. 1.1 Closed-cycle, nuclear MHD conversion system.

2 PROJECT DESCRIPTION

This section is based on the contents of paragraph 4.2 in the Statement of Work.

The work is divided into four tasks.

Task 1. Reflector Modeling

This task shall provide the nuclear analysis of the concept, performed on a reference PCU geometry, using developed and open computer codes available at ANSALDO.

The reflector modeling shall address the following items:

- Reflector reactivity worth.
- Power density distribution inside the PCU, at constant core power level.

Task 2. Working Fluid Characteristics

This task shall provide an analytical model enabling the prediction of the temperature distribution and ionization levels of the working fluid in the PCU.

Since the equilibrium thermal ionization is not expected to maintain sufficient electrical conductivity for efficient power generation, this task shall investigate additional ionization mechanisms that can be present in a fissioning plasma.

Task 3. Electrical Conductivity Effects

This task shall provide appropriate relations enabling the prediction of the electrical conductivity of the working gas. For this purpose, this task shall primarily address the evaluation of the electron mobility in the gas. The possible contribution (beneficial and/or detrimental) to electric conductivity of the other charged particles in the gas, such as F- ions, shall be taken into account.

Task 4. Reporting

This task concerns the execution of the reporting requirements incorporated in the contract.

1 REFLECTOR MODELING

1.1 Symbols, Terms and Abbreviations

a	Absorption
a/o	Atom per cent
BOL	Beginning of life
BU	Fuel burn-up
CZP	Cold zero power
f	Fission
HFP	Hot full power
HZP	Hot zero power
g	Energy group
pcm	Percent mille (a reactivity change of 1 pcm equals a reactivity change of 10e-5 $\Delta\rho$)
Power density	The thermal power produced per unit volume of the core (W/cm^3)
ρ	Reactivity
$\Delta\rho$	Change in reactivity, defined as $\Delta\rho = \ln(k2/k1)$, where k1 and k2 are the eigenvalues obtained from two calculations that differ only in the values assigned to the independent variables
r	Removal

shutdown margin	The amount of negative reactivity (ρ) by which a reactor is maintained in subcritical state at CZP conditions after a control trip
Teff	Resonance effective temperature of the fuel
tr	Transport

3.2 Reference Core Description

General

The results presented in this section are referred to the reactor reference configuration shown in Figures 3.1-3.2.

This configuration is a simplified arrangement subject to the limitations of the codes adopted in the analysis: in particular, a coarse discretization of both composition and geometry has been made at the core inlet and outlet conical segments.

A simple axial-inlet flow pattern has been adopted in the analysis: however, the cooling requirements of the wall made it necessary to add an internal diffuser that divides the inlet flow into two parts, the larger flowing in the annulus between the internal diffuser and the external one.

In this reactor the same fluid acts as working medium and fuel: it flows across the reactor cavity and consists of highly enriched gaseous UF6 (region 1 of Fig. 3.1): 90% a/o enriched in U235 with the reactor at BOL.

The core supplies a thermal power of 277 Mw at full power.

The following parameters have been fixed for the power density distribution calculations inside the core and for the reactivity integral worth evaluation of the movable reflector:

- Reactor at full power (HFP),
- BOL,
- no xenon, no Sm,
- inlet pressure 15 MPa,
- UF6 flow rate 1000 kg/s,
- inlet temperature 1720 K.

The rationale for the selection of these system parameters is provided in section 5.2.

Besides, in order to estimate the reactivity requirements during reactor operations, two additional core conditions have been defined:

a) condition I:

- Core at cold zero power (CZP),
- BOL,
- UF6 inlet pressure 52 bar,
- UF6 inlet temperature 573 K,
- UF6 flow rate 1000 kg/s,

b) condition II:

- Core at not zero power (HZP),
- BOL,
- UF6 inlet pressure 15 MPa,
- UF6 inlet temperature 1720 K,
- UF6 flow rate 1000 kg/s,

The above conditions are possible if the reactor control system can assure that:

A) condition I is reached without using nuclear heating to attain the gaseous phase of the fuel;

B) the fuel density at the core inlet is kept constant (0.36 g/cm^3) by controlling the inlet parameters during reactor operations.

Components

The dimensions of the reactor components (shown in Figures 3.1-3.2) have been fixed after some preliminary considerations, based on the thermal and mechanical feasibility of the system and on the basic neutronic requirements enabling the core reactivity to be controlled by a movable reflector, sliding axially on the external side of the pressure vessel.

As already pointed out in [1], the main problem is the selection of a pressure vessel material highly transparent to neutrons.

It can be shown that the adoption of the most common metallic materials , such as nickel alloys or stainless-steel, introduces a strong reactivity penalty and decouples the inner shells from the external movable reflector to such a degree that reflector worth becomes negligible.

For the above reasons a Zr/Nb alloy (UNS=R60901) has been finally selected as pressure vessel material.

The cylindrical shell thickness (10 cm) has been evaluated preliminarily in conformity with the ASME III Code [2] for a permanent static load condition at 15 MPa. In order to minimize creep phenomena the pressure vessel maximum temperature has been supposed to be lower than 620 K.

To keep the pressure vessel temperature at such a low value an active heat removal system has to be provided.

Since the maximum temperature in the reactor cavity is expected to reach about 2800 K close to the wall, highly refractory materials have been used: in particular, a graphite shell (10 cm thick) and a BeO shell (10 cm thick) have been interposed between the fuel and the pressure vessel.

These shells have to be cooled by helium gas flowing across a number of coolant channels obtained in the shells themselves.

The purpose of the coolant system is twofold:

1) to remove the gamma and neutron heating from the inner shells:

2) to create a strong temperature gradient between fuel and pressure vessel. Tab. 3.1 shows the radial temperature profile assumed for the core reference configuration.

Furthermore, in order to avoid the corrosion reactions between UF6 and graphite, a thin Mo-alloy liner (0.6 mm thick) has been placed to insulate the fuel from the graphite surface.

An adequate liner material is TZM (UNS=P/M,R03640) that has a high melting point (3300 K) and a liquidus temperature at 2895 K.

Typical fields of application of this material are heat engines, extrusion dies and nuclear reactors, as it retains good mechanical performances at high temperature.

It should be pointed out that only Mo-alloys can be probably used for structural parts in the reactor cavity (e.g. the diffuser); however, since these alloys act as strong absorbers in the proposed concept of gas reactor, their use should be limited.

In this preliminary feasibility analysis, however, the internals (diffuser and gas coolant tubes) have been ignored: the reactivity penalty due to the internal materials can be balanced by increasing fuel enrichment.

Finally, beryllium has been selected as the material of the movable reflector.

Mass and volume of the reactor components are summarized in Tab. 3.2.

3.3 Analysis Codes

The principal computer codes adopted in the analysis are GGC-4 [3] (zero-dimensional), ANISN [4] (one-dimensional), SQUID-360 [5] (two-dimensional), WAPITI-GAS [6] (two-dimensional), MERCURE-IV [7] (three-dimensional). A brief presentation of these codes is provided below: additional information can be found in the references.

GGC-4 Code:

GGC-4 is a point model neutron spectrum program.

The fast and thermal spectrum calculations are performed by the methods of GAM [8] and GATHER [9], respectively.

Input microscopic cross section data are based on the ENDF/B-IV Library [10]

The energy range is divided into a number of fast groups (up to 99) and thermal groups (up to 101).

ANISN Code :

ANISN solves the one-dimensional Boltzmann transport equation for slabs, and for cylindrical or spherical geometries.

As secondary calculation, the detailed flux generated as the solution of the Boltzmann equation may be used to perform a group reduction of the cross sections.

SQUID-360 Code:

SQUID is a multigroup finite difference diffusion code in two dimensions (X-Y or R-Z).

WAFITI-GAS Code:

WAFITI-GAS is a finite difference code developed by ANSALDO for two-dimensional (X-Y or R-Z) thermal-fluid analysis of compressible systems. It is derived from the French code WAFITI.

MERCURE-IV Code:

The Monte Carlo code MERCURE-IV computes in a three-dimensional heterogeneous geometry heating and gamma dose rates, and by the point-wise kernel attenuation in a straight line, the fast fluxes.

Tabulated accumulation factors give the contribution of the scattered gamma rays. The program calculates the accumulation factors for mixtures; for multi-layer media the Kitazume formulation is used.

Additional support codes have been used for special calculations such as the correlation factors and the cross section update during the iteration process between SDUID and WAFITI.

3.4 Features of Performed Calculations

<u>Fuel and structural material cross sections</u>

In accordance with the scheme reported in Fig. 3.3 the cross sections have been calculated by using:

a) GGC-4 for the fuel cross sections with:

- fast energy range from 14.9 MeV to 2.38 eV and B1 approximation (GAM);
- thermal energy range from 2.38 eV to zero and B0 approximation (GATHER);

- 50 group microscopic cross section generation (41 fast groups and 9 thermal groups) to be input to ANISN code in order to generate fuel and structural cross sections.
  The assumed energy cuts are shown in Tab. 3.3.

b) GGC-4 as in item a) but for the structural cross sections with:

- B1 approximation in GATHER.

c) ANISN code using cylindrical geometry and P0-S4 approximation in order to:

- investigate the fuel 5 group cross section dependence on the temperature and density of the fuel;
- generate the structural material macroscopic cross sections and a 5 group cross section data set to calculate the fuel macroscopic cross sections to be input to SQUID code as a function of temperature and density at each iteration step.

The assumed energy cuts in the range 14.9 MeV - 0.0 eV are 14.9 MeV, 0.821 MeV, 150 keV, 5.53 keV, 0.625 eV, 0.0 eV.

Reactor Calculations

In accordance with the scheme reported in Fig. 3.4, total reflector worth and the distributions of thermal power, fuel temperature, and fuel density have been calculated by using:

a) SQUID-360 code with:

- simplified R-Z geometry and material compositions,
- k-eff calculation,
- spatial fluxes calculations in order to evaluate the thermal power density distribution to be input to WAPITI code.

b) WAPITI-GAS code for the thermal-fluid analysis with:

- R-Z geometry,
- turbulent flow,
- density and temperature distributions of the fuel to be input to SQUID-360 Code.

3.5 Nuclear Cross Section Calculations

The macroscopic cross sections required as input data for the full core R-Z SQUID calculations have been generated by using the procedure outlined in Fig. 3.3. The cross sections are referred to :

-fuel,

-structural material.

Fuel cross sections

It has been assumed that inside the reference core configuration (see par. 3.1) fuel temperature and density may change in the range 1800-3000 K and 0.15-0.45 g/cm^3, respectively, as shown in Fig. 3.5.

A sensitivity analysis has been performed by applying the procedure of Fig. 3.3 to each of the points 1-9 of Fig. 3.5.

The results are summarized below:

a) the fuel microscopic cross sections change only:
   - with fuel density in the 4th energetic group (epithermal range),
   - with fuel temperature in the 5th energetic group (thermal group);

b) the 5 group structural material cross sections are not significantly affected by the fuel conditions under the assumption that the radial temperature profile in the structural material doesn't change.

Consequently, in order to update the fuel macroscopic cross sections during the iterative SOUID calculations of reactor power distribution with thermal-fluid feedback, the following correlations can be used:

$$\Sigma_j^g(T,n) = \Sigma_j^g(To,no)\frac{n}{no} \qquad \begin{array}{l} g=1,3 \text{ and } j=tr,a,f \\ \text{or} \\ g=1,4 \text{ and } j=r \end{array}$$

$$\Sigma_j^4(T,n) = \Sigma_j^4(To,no)\frac{n}{no} + \Delta\Sigma_j^4(n) \qquad j=tr,a,f$$

$$\Sigma_j^5(T,n) = \Sigma_j^5(To,no)\frac{n}{no} + \Delta\Sigma_j^5(T) \qquad j=tr,a,f$$

$$\Delta\Sigma_j^4(n) = n(a_j n^2 + b_j n + c_j) \qquad j=tr,a,f$$

$$\Delta\Sigma_j^5(T) = n(A_j T^2 + B_j T + C_j)$$

where:

$[n]=g/cm^3$ $[T]=K$, $no=0.3\ g/cm^3$ $To=2100\ K$

The correlation coefficients a_j, b_j, c_j, A_j, B_j, C_j have been estimated by using the previous ANISN calculations.

The results are reported in Tab. 3.4.

Structural material cross sections

The structural macroscopic cross sections for the full core R-Z SQUID calculations have been evaluated by ANISN with the procedure shown in Fig. 3-3 by fixing fuel density at 0.30 g/cm^3 and fuel temperature at 2100 K, which represent average values in the core reference configuration.

3.6 Reactor Calculations

The reactor calculations have been performed by applying the scheme reported in Fig. 3.4 to the core reference configuration with:

a) external reflector out, 65% of the fuel flowing in the annular diffuser and 35% of the fuel flowing in the internal diffuser;

b) as in item a), but with the external reflector 100% in;

c) external reflector 100% in, 70% of the fuel flowing in the annular diffuser and 30% of the fuel flowing in the internal diffuser.

The proposed scheme can be useful to study a generic stationary core configuration in order to evaluate power density distribution and k-effective, along with fuel temperature and density distributions.

In short, the calculation procedure is the following:

1) a guess power density distribution is fixed,

2) WAFITI-GAS computes the fuel density and temperature distributions generated by the input power density distribution.

3) the fuel density and temperature distributions are used to update the nuclear macroscopic cross sections for each fuel composition.

4) SQUID computes a new power density distribution and eigenvalue,

5) a test on the convergence of the main variables is made: if it is successful, than the iterative process is stopped: if not, it returns to step 2).

Figures 3.6-3.8 report the axial profile of power density at different radii for the above configurations.

Tables 3.5-3.7 show the respective temperature distributions in the reactor cavity. The values are computed at the center of each mesh. The axial coordinate is given in the first column of the table, the value at the top corresponding to the reactor inlet: radially, the mesnes are numbered from the reactor axis.

3.7 Reactivity Requirements

In this core concept, excess reactivity is controlled by the external movable reflector. This excess reactivity includes:

a) reactivity changes due to changes in gas working temperature between the cold and hot, no load conditions:

b) reactivity changes due to changes in reactor power over the power range of operations;

c) reactivity changes due to fuel depletion;

d) reactivity associated to the minimum shutdown margin.

The reactivity change associated to each item is reported in Tab. 3.8.

The integral worth of the movable reflector has been evaluated by means of the reactor calculations: an uncertainty of about 10% has been associated to the results.

The reactivity change between CZF and hZF does not appear to be significant because in this reactor the Doppler effect has been considered only for UII8, as in the GAM library there isn't any information about the Doppler effect in UII5.

Finally, since it is not in the scope of this preliminary analysis to make accurate assumptions about the system operating modes, it has been supposed that the reactor is operated at full power level continuosly.

It has been estimated that, with a 3300 pcm of reactivity change available for depletion, reactor life is limited to a few hours because of the strong Xenon poisoning that affects this type of core. This time is a function of the UFo overall plant/core mass ratio as shown in Fig. 3.9.

The full power level can be restored after an interval of time whose length depends on the operational strategy; the process can be repeated until fuel depletion allows it.

Fig 3.10 shows the evolution of reactivity after a shutdown performed at the end of the first lifetime at full power, whose length is about 5 hours. In this case, which is referred to a UF_6 mass ratio of 5, the time required for reactivity to become positive again is approximately 30 hours from shutdown; this waiting time is reduced by increasing the mass ratio.

The minimum value of reactivity that occurs 9 hours after shutdown in Fig. 3.10, corresponding to a maximum of the Xe concentration, is explained by the presence of a source of Xe135, the radioactive decay of I135, in competition with its disappearance due to decay to Cs135.

3.8 References

[1] ANSALDO SpA, "Nuclear MHD Converter", Semi-Annual Technical Progress Report, RD-06-04-SAPR, November 1988.

[2] "ASME Boiler and Pressure Vessel Code", Nuclear Power Plant Components Division 1.

[3] Adir J. and Lathrop K.D., "Theory of Methods used in the GGC-4 Multigroup Cross Sections Code", GA-9021 October 1968.

[4] ANISN-ORNL CCC/254, "Multigroup One-Dimensional Discrete Ordinates Transport Code with Anisotropic Scattering".

[5] Daneri A., Gabutti B., Salina E. "SOUID-360 - A Multigroup Diffusion Program with Criticality Searches for the IBM-360", EUR 3882e 1968.

[6] CEA - DTCE/STT, "Programme WAPITI, Notice de présentation", Déscriptif informatique n.ro 90187 - Rev. 0, 18-3-1981.

[7] Devillers C. and Dupont C., "Mercure-IV, un programme de Monte Carlo a trois dimensions pour l'integration de noyaux punctuel d'attenuation en ligne droite", Report SERMA - T - 496 1980.

[8] Joanou G.D.D. and Dudek J.S., "GAM-II-A B3 Code for the Calculation of Fast Neutron Spectrum and Associated Multigroup Constants", GA - 4265 September 1963.

[9] G.D. Joanou et al., "GATHER-II, An IBM 7090 Fortran-II Program for the Computation of Thermal-Neutron Spectra and Associated Multigroup Cross Sections", GA-4132 1963.

[10] Ozer O. and Garber D., "ENDF/B Summary Documentation, ENDF-201", BNL 17451, Brookhaven National Laboratory, Upton New York, 1973.

Tab. 3.1 Radial temperature profile in the core reference configuration.

Radial Range (*) (cm)	Material	Average Temperature (K)
50.0-53.5	Graphite	2200
53.5-56.5	"	1500
56.5-60.0	"	1200<T<1500
60.0-63.5	BeO	900<T<1200
63.5-66.0	"	900
66.0-70.0	"	600<T<900
70.0-80.0	Zr-Nb	<600
80.0-110.0	Be	<600

(*)see Fig. 3.1

Tab. 3.2 Mass and volume summary for the core reference configuration.

Reactor Material	Average Density (kg/dm3)	Volume (dm3)	Mass (kg)	% of Total Mass
UF6	0.29	1723	500	1.9
TZM	10.16	2.93	29	0.1
Graphite	1.71	1320	2257	8.5
BeO	3.02	1317	3977	14.9
Zr-Nb alloy	6.5	1634	10621	39.8
Be	1.85	5012	9272	34.8
Total Reactor Mass			26656	100.0

Tab. 3.3 50 group energy cuts in the CCC-4 calculations

TEAST PROBLEM NO 1.

BROAD GROUP	STRUCTURE FOR THIS PROBLEM ENERGY INTERVAL (E V)		
1	1.491825E+07	TO	1.105171E+07
2	1.105171E+07	TO	8.187308E+06
3	8.187308E+06	TO	6.703200E+06
4	6.703200E+06	TO	5.488116E+06
5	5.488116E+06	TO	4.493290E+06
6	4.493290E+06	TO	3.678795E+06
7	3.678795E+06	TO	2.725318E+06
8	2.725318E+06	TO	2.018965E+06
9	2.018965E+06	TO	1.353353E+06
10	1.353353E+06	TO	1.002589E+06
11	1.002589E+06	TO	8.208501E+05
12	8.208501E+05	TO	4.978708E+05
13	4.978708E+05	TO	3.337328E+05
14	3.337328E+05	TO	2.237078E+05
15	2.237078E+05	TO	1.499558E+05
16	1.499558E+05	TO	8.651700E+04
17	8.651700E+04	TO	4.086773E+04
18	4.086773E+04	TO	1.503140E+04
19	1.503140E+04	TO	5.530848E+03
20	5.530848E+03	TO	2.034684E+03
21	2.034684E+03	TO	9.611169E+02
22	9.611169E+02	TO	5.829468E+02
23	5.829468E+02	TO	3.535752E+02
24	3.535752E+02	TO	2.144542E+02
25	2.144542E+02	TO	1.300730E+02
26	1.300730E+02	TO	1.013010E+02
27	1.013010E+02	TO	7.889328E+01
28	7.889328E+01	TO	6.144214E+01
29	6.144214E+01	TO	4.785120E+01
30	4.785120E+01	TO	3.726654E+01
31	3.726654E+01	TO	2.902321E+01
32	2.902321E+01	TO	2.260330E+01
33	2.260330E+01	TO	1.760347E+01
34	1.760347E+01	TO	1.370960E+01
35	1.370960E+01	TO	1.067704E+01
36	1.067704E+01	TO	8.315291E+00
37	8.315291E+00	TO	6.475955E+00
38	6.475955E+00	TO	5.043479E+00
39	5.043479E+00	TO	3.927865E+00
40	3.927865E+00	TO	3.059024E+00
41	3.059024E+00	TO	2.382371E+00

PROBLEMAL PROBLEM NO 1.
ENERGY EV

BROAD GROUP	UPPER LIMIT	LOWER LIMIT
1	2.3800	1.860
2	1.8600	1.440
3	1.4400	.876
4	.8760	.683
5	.6830	.414
6	.4140	.100
7	.1000	.025
8	.0253	.008
9	.0080	0.0

Tab. 3.4 Correlation coefficients for the macroscopic cross section update.

for	aj	bj	cj
$\tilde{\sigma}_{tr}$	.57058-08	-.18493-04	.13976-01
$\tilde{\sigma}_{f}$	.11165-07	-.36495-04	.27717-01
$\tilde{\sigma}_{a}$	.56746-08	-.18385-04	.13891-01

for	AJ	BJ	CJ
$\tilde{\sigma}_{tr}$	.75159-01	-.79930-01	.17589-01
$\tilde{\sigma}_{f}$	.89438-01	-.93414-01	.20401-01
$\tilde{\sigma}_{a}$	.58139-01	-.60523-01	.13199-01

TEMPERATURES
****

JC	-Z-	1	2	3	4	5	6	7	8
18	2.738	.1451E+04	.1451E+04	.1451E+04	.1451E+04	.1451E+04	.0000E+00	.0000E+00	.0000E+00
17	2.613	.1456E+04	.1456E+04	.1456E+04	.1455E+04	.1455E+04	.1459E+04	.0000E+00	.0000E+00
16	2.488	.1461E+04	.1461E+04	.1462E+04	.1506E+04	.1460E+04	.1464E+04	.1509E+04	.1648E+04
15	2.363	.1467E+04	.1467E+04	.1469E+04	.1515E+04	.1466E+04	.1469E+04	.1489E+04	.1499E+04
14	2.225	.1474E+04	.1474E+04	.1480E+04	.1567E+04	.1652E+04	.1480E+04	.1499E+04	.1515E+04
13	2.075	.1482E+04	.1482E+04	.1492E+04	.1558E+04	.1605E+04	.1494E+04	.1504E+04	.1516E+04
12	1.913	.1492E+04	.1493E+04	.1508E+04	.1566E+04	.1605E+04	.1622E+04	.1536E+04	.1546E+04
11	1.725	.1504E+04	.1508E+04	.1532E+04	.1588E+04	.1626E+04	.1638E+04	.1594E+04	.1597E+04
10	1.525	.1517E+04	.1525E+04	.1558E+04	.1613E+04	.1650E+04	.1669E+04	.1648E+04	.1651E+04
9	1.325	.1530E+04	.1544E+04	.1585E+04	.1638E+04	.1675E+04	.1701E+04	.1699E+04	.1709E+04
8	1.125	.1545E+04	.1566E+04	.1612E+04	.1664E+04	.1702E+04	.1735E+04	.1749E+04	.1772E+04
7	.925	.1563E+04	.1590E+04	.1639E+04	.1692E+04	.1733E+04	.1772E+04	.1802E+04	.1844E+04
6	.738	.1581E+04	.1613E+04	.1667E+04	.1724E+04	.1771E+04	.1818E+04	.1869E+04	.1935E+04
5	.575	.1602E+04	.1642E+04	.1705E+04	.1775E+04	.1837E+04	.1904E+04	.1989E+04	.2086E+04
4	.438	.1642E+04	.1688E+04	.1773E+04	.1870E+04	.1959E+04	.2049E+04	.2159E+04	.2264E+04
3	.313	.1697E+04	.1785E+04	.1903E+04	.2028E+04	.2124E+04	.2198E+04	.2267E+04	.2331E+04
2	.188	.1784E+04	.1895E+04	.2022E+04	.2122E+04	.2173E+04	.2209E+04	.0000E+00	.0000E+00
1	.063	.1797E+04	.1909E+04	.2033E+04	.2129E+04	.0000E+00	.0000E+00	.0000E+00	.0000E+00

JC	-Z-	9	10	11	12	13	14	15
18	2.738	.0000E+00	.0000E+00	.0000E+00	.0000E+00	.0000E+00	.0000E+00	.0000E+00
17	2.613	.0000E+00	.0000E+00	.0000E+00	.0000E+00	.0000E+00	.0000E+00	.0000E+00
16	2.488	.0000E+00	.0000E+00	.0000E+00	.0000E+00	.0000E+00	.0000E+00	.0000E+00
15	2.363	.1534E+04	.1643E+04	.0000E+00	.0000E+00	.0000E+00	.0000E+00	.0000E+00
14	2.225	.1550E+04	.1634E+04	.1847E+04	.1832E+04	.0000E+00	.0000E+00	.0000E+00
13	2.075	.1538E+04	.1577E+04	.1644E+04	.1683E+04	.1771E+04	.2039E+04	.0000E+00
12	1.913	.1574E+04	.1624E+04	.1698E+04	.1763E+04	.1822E+04	.1972E+04	.2142E+04
11	1.725	.1636E+04	.1707E+04	.1796E+04	.1878E+04	.1927E+04	.2033E+04	.2181E+04
10	1.525	.1702E+04	.1791E+04	.1894E+04	.1982E+04	.2028E+04	.2101E+04	.2208E+04
9	1.325	.1770E+04	.1877E+04	.1985E+04	.2072E+04	.2113E+04	.2167E+04	.2245E+04
8	1.125	.1847E+04	.1960E+04	.2068E+04	.2150E+04	.2187E+04	.2230E+04	.2290E+04
7	.925	.1930E+04	.2046E+04	.2151E+04	.2226E+04	.2258E+04	.2293E+04	.2342E+04
6	.738	.2032E+04	.2142E+04	.2236E+04	.2302E+04	.2328E+04	.2357E+04	.2397E+04
5	.575	.2194E+04	.2293E+04	.2369E+04	.2415E+04	.2429E+04	.2458E+04	.2492E+04
4	.438	.2353E+04	.2419E+04	.2477E+04	.2530E+04	.0000E+00	.0000E+00	.0000E+00
3	.313	.2391E+04	.0000E+00	.0000E+00	.0000E+00	.0000E+00	.0000E+00	.0000E+00
2	.188	.0000E+00	.0000E+00	.0000E+00	.0000E+00	.0000E+00	.0000E+00	.0000E+00
1	.063	.0000E+00	.0000E+00	.0000E+00	.0000E+00	.0000E+00	.0000E+00	.0000E+00

Tab. 3.5 Temperature distribution in the reactor cavity. External reflector 100% in and 65% of the fuel through the annular diffuser.

TEMPERATURES
****

JC	Z-	1	2	3	4	5	6	7	8
18	2.738	.1452E+04	.1452E+04	.1452E+04	.1451E+04	.1451E+04	.0000E+00	.0000E+00	.0000E+00
17	2.613	.1457E+04	.1457E+04	.1457E+04	.1456E+04	.1456E+04	.1460E+04	.0000E+00	.0000E+00
16	2.488	.1463E+04	.1463E+04	.1464E+04	.1514E+04	.1462E+04	.1466E+04	.1518E+04	.1676E+04
15	2.363	.1469E+04	.1469E+04	.1471E+04	.1528E+04	.1468E+04	.1472E+04	.1494E+04	.1506E+04
14	2.225	.1477E+04	.1477E+04	.1484E+04	.1579E+04	.1471E+04	.1484E+04	.1505E+04	.1524E+04
13	2.075	.1485E+04	.1486E+04	.1496E+04	.1569E+04	.1618E+04	.1499E+04	.1510E+04	.1524E+04
12	1.913	.1496E+04	.1497E+04	.1514E+04	.1577E+04	.1618E+04	.1636E+04	.1545E+04	.1556E+04
11	1.725	.1509E+04	.1513E+04	.1539E+04	.1599E+04	.1638E+04	.1650E+04	.1604E+04	.1608E+04
10	1.525	.1521E+04	.1530E+04	.1565E+04	.1623E+04	.1661E+04	.1680E+04	.1659E+04	.1662E+04
9	1.325	.1535E+04	.1550E+04	.1592E+04	.1647E+04	.1685E+04	.1711E+04	.1709E+04	.1718E+04
8	1.125	.1550E+04	.1571E+04	.1619E+04	.1672E+04	.1711E+04	.1743E+04	.1757E+04	.1779E+04
7	9.	.1567E+04	.1595E+04	.1646E+04	.1699E+04	.1740E+04	.1778E+04	.1808E+04	.1849E+04
6	.738	.1585E+04	.1618E+04	.1673E+04	.1730E+04	.1776E+04	.1823E+04	.1872E+04	.1937E+04
5	.575	.1606E+04	.1647E+04	.1711E+04	.1780E+04	.1841E+04	.1907E+04	.1990E+04	.2085E+04
4	.438	.1636E+04	.1693E+04	.1777E+04	.1873E+04	.1961E+04	.2049E+04	.2157E+04	.2260E+04
3	.313	.1701E+04	.1789E+04	.1906E+04	.2029E+04	.2124E+04	.2197E+04	.2265E+04	.2328E+04
2	.188	.1788E+04	.1898E+04	.2023E+04	.2122E+04	.2172E+04	.2206E+04	.0000E+00	.0000E+00
1	.063	.1801E+04	.1912E+04	.2034E+04	.2129E+04	.0000E+00	.0000E+00	.0000E+00	.0000E+00

JC	Z-	9	10	11	12	13	14	15
18	2.738	.0000E+00	.0000E+00	.0000E+00	.0000E+00	.0000E+00	.0000E+00	.0000E+00
17	2.613	.0000E+00	.0000E+00	.0000E+00	.0000E+00	.0000E+00	.0000E+00	.0000E+00
16	2.488	.0000E+00	.0000E+00	.0000E+00	.0000E+00	.0000E+00	.0000E+00	.0000E+00
15	2.363	.1545E+04	.1668E+04	.0000E+00	.0000E+00	.0000E+00	.0000E+00	.0000E+00
14	2.225	.1563E+04	.1655E+04	.1886E+04	.1865E+04	.0000E+00	.0000E+00	.0000E+00
13	2.075	.1548E+04	.1591E+04	.1663E+04	.1705E+04	.1798E+04	.2080E+04	.0000E+00
12	1.913	.1586E+04	.1640E+04	.1719E+04	.1789E+04	.1851E+04	.2009E+04	.2186E+04
11	1.725	.1650E+04	.1724E+04	.1817E+04	.1902E+04	.1957E+04	.2068E+04	.2222E+04
10	1.525	.1714E+04	.1806E+04	.1911E+04	.2003E+04	.2054E+04	.2131E+04	.2242E+04
9	1.325	.1781E+04	.1889E+04	.1998E+04	.2088E+04	.2134E+04	.2191E+04	.2272E+04
8	1.125	.1855E+04	.1968E+04	.2077E+04	.2161E+04	.2202E+04	.2248E+04	.2310E+04
7	.925	.1935E+04	.2051E+04	.2155E+04	.2232E+04	.2268E+04	.2306E+04	.2356E+04
6	.738	.2033E+04	.2142E+04	.2236E+04	.2303E+04	.2334E+04	.2366E+04	.2408E+04
5	.575	.2192E+04	.2292E+04	.2369E+04	.2417E+04	.2436E+04	.2468E+04	.2503E+04
4	.438	.2349E+04	.2414E+04	.2472E+04	.2524E+04	.0000E+00	.0000E+00	.0000E+00
3	.313	.2388E+04	.0000E+00	.0000E+00	.0000E+00	.0000E+00	.0000E+00	.0000E+00
2	.188	.0000E+00	.0000E+00	.0000E+00	.0000E+00	.0000E+00	.0000E+00	.0000E+00
1	.063	.0000E+00	.0000E+00	.0000E+00	.0000E+00	.0000E+00	.0000E+00	.0000E+00

Tab. 3.6 Temperature distribution in the reactor cavity.
External reflector out and 65% of the fuel through
the annular diffuser.

TEMPERATURES
****

JC	-Z-	1	2	3	4	5	6	7	8
18	2.738	.1452E+04	.1452E+04	.1452E+04	.1451E+04	.1451E+04	.0000E+00	.0000E+00	.0000E+00
17	2.613	.1457E+04	.1457E+04	.1457E+04	.1454E+04	.1454E+04	.1458E+04	.0000E+00	.0000E+00
16	2.488	.1463E+04	.1463E+04	.1464E+04	.1514E+04	.1459E+04	.1463E+04	.1504E+04	.1634E+04
15	2.363	.1470E+04	.1470E+04	.1472E+04	.1523E+04	.1465E+04	.1467E+04	.1485E+04	.1495E+04
14	2.225	.1478E+04	.1478E+04	.1485E+04	.1576E+04	.1676E+04	.1478E+04	.1494E+04	.1510E+04
13	2.075	.1487E+04	.1488E+04	.1498E+04	.1567E+04	.1615E+04	.1490E+04	.1499E+04	.1510E+04
12	1.913	.1499E+04	.1500E+04	.1516E+04	.1577E+04	.1627E+04	.1698E+04	.1534E+04	.1538E+04
11	1.725	.1513E+04	.1517E+04	.1540E+04	.1604E+04	.1643E+04	.1652E+04	.1593E+04	.1584E+04
10	1.525	.1528E+04	.1537E+04	.1573E+04	.1632E+04	.1669E+04	.1680E+04	.1648E+04	.1635E+04
9	1.325	.1545E+04	.1560E+04	.1604E+04	.1661E+04	.1697E+04	.1714E+04	.1698E+04	.1689E+04
8	1.125	.1561E+04	.1586E+04	.1636E+04	.1691E+04	.1727E+04	.1750E+04	.1747E+04	.1747E+04
7	.925	.1584E+04	.1614E+04	.1668E+04	.1723E+04	.1761E+04	.1788E+04	.1798E+04	.1814E+04
6	.738	.1606E+04	.1642E+04	.1701E+04	.1760E+04	.1800E+04	.1833E+04	.1859E+04	.1898E+04
5	.575	.1632E+04	.1679E+04	.1747E+04	.1814E+04	.1865E+04	.1911E+04	.1966E+04	.2035E+04
4	.438	.1671E+04	.1733E+04	.1817E+04	.1900E+04	.1968E+04	.2030E+04	.2108E+04	.2184E+04
3	.313	.1740E+04	.1826E+04	.1929E+04	.2025E+04	.2094E+04	.2145E+04	.2195E+04	.2242E+04
2	.188	.1820E+04	.1918E+04	.2020E+04	.2095E+04	.2143E+04	.2156E+04	.0000E+00	.0000E+00
1	.063	.1833E+04	.1931E+04	.2030E+04	.2102E+04	.0000E+00	.0000E+00	.0000E+00	.0000E+00

JC	-Z-	9	10	11	12	13	14	15
18	2.738	.0000E+00	.0000E+00	.0000E+00	.0000E+00	.0000E+00	.0000E+00	.0000E+00
17	2.613	.0000E+00	.0000E+00	.0000E+00	.0000E+00	.0000E+00	.0000E+00	.0000E+00
16	2.488	.0000E+00	.0000E+00	.0000E+00	.0000E+00	.0000E+00	.0000E+00	.0000E+00
15	2.363	.1527E+04	.1625E+04	.0000E+00	.0000E+00	.0000E+00	.0000E+00	.0000E+00
14	2.225	.1541E+04	.1615E+04	.1797E+04	.1836E+04	.0000E+00	.0000E+00	.0000E+00
13	2.075	.1529E+04	.1563E+04	.1619E+04	.1652E+04	.1723E+04	.1920E+04	.0000E+00
12	1.913	.1559E+04	.1597E+04	.1656E+04	.1712E+04	.1753E+04	.1860E+04	.1960E+04
11	1.725	.1610E+04	.1664E+04	.1739E+04	.1808E+04	.1831E+04	.1911E+04	.2020E+04
10	1.525	.1666E+04	.1736E+04	.1822E+04	.1896E+04	.1914E+04	.1972E+04	.2065E+04
9	1.325	.1725E+04	.1809E+04	.1904E+04	.1975E+04	.1993E+04	.2035E+04	.2106E+04
8	1.125	.1791E+04	.1884E+04	.1981E+04	.2049E+04	.2066E+04	.2098E+04	.2152E+04
7	.925	.1870E+04	.1965E+04	.2059E+04	.2123E+04	.2136E+04	.2161E+04	.2203E+04
6	.738	.1969E+04	.2060E+04	.2141E+04	.2193E+04	.2202E+04	.2222E+04	.2255E+04
5	.575	.2116E+04	.2195E+04	.2253E+04	.2283E+04	.2285E+04	.2305E+04	.2333E+04
4	.438	.2252E+04	.2304E+04	.2350E+04	.2393E+04	.0000E+00	.0000E+00	.0000E+00
3	.313	.2289E+04	.0000E+00	.0000E+00	.0000E+00	.0000E+00	.0000E+00	.0000E+00
2	.188	.0000E+00	.0000E+00	.0000E+00	.0000E+00	.0000E+00	.0000E+00	.0000E+00
1	.063	.0000E+00	.0000E+00	.0000E+00	.0000E+00	.0000E+00	.0000E+00	.0000E+00

Tab. 3.7 Temperature distribution in the reactor cavity.
External reflector 100% in and 70% of the fuel
through the annular diffuser.

Tab. 3.8 Reactivity balance for the core reference configuration.

Movable reflector integral worth	9.6%
Assumed uncertainty (10%)	-0.96%
From HZP to HFP	-4.3%
From CZP to HZP	0%
Shutdown margin plus depletion	4.34%

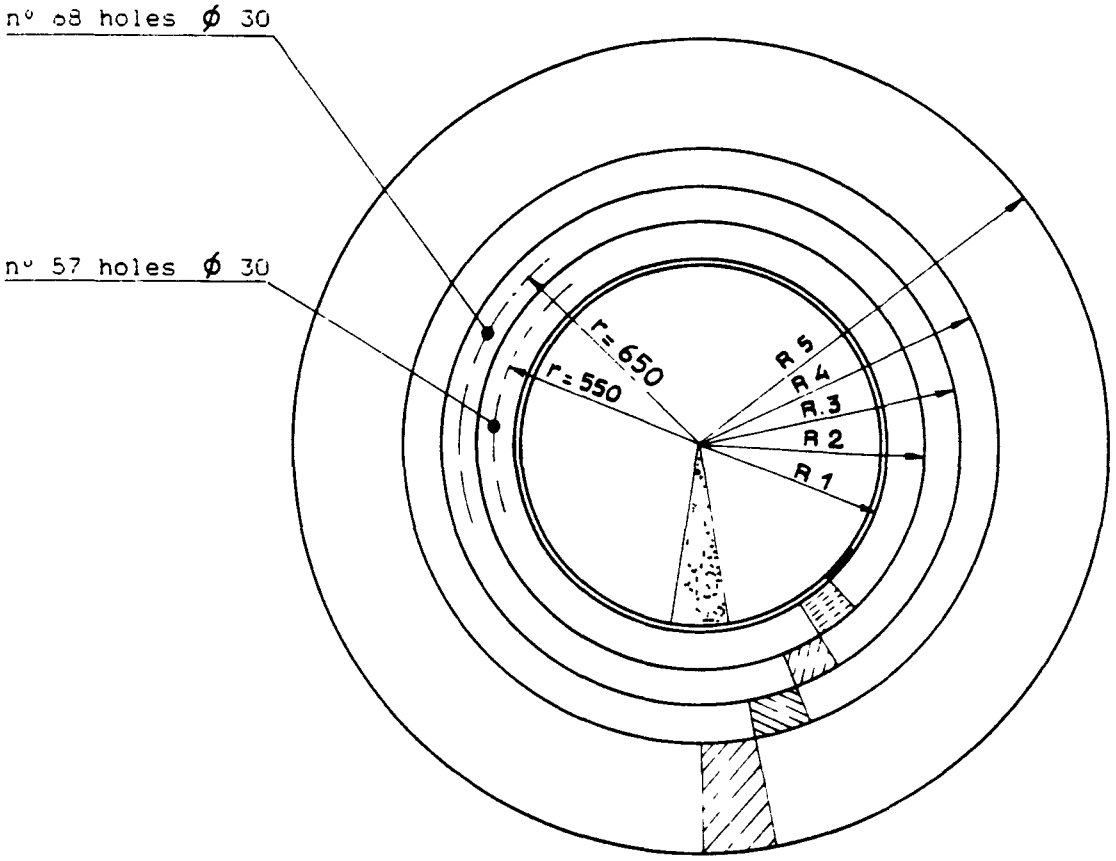

1 20

Arrow N°	Nominal radius (mm)	Material
		UFo
1	1000	TZM
2	1200	Graphite
3	1400	BeO
4	1600	Zr-Nb alloy
5	2200	Be

Fig. 3.1 Core cross section

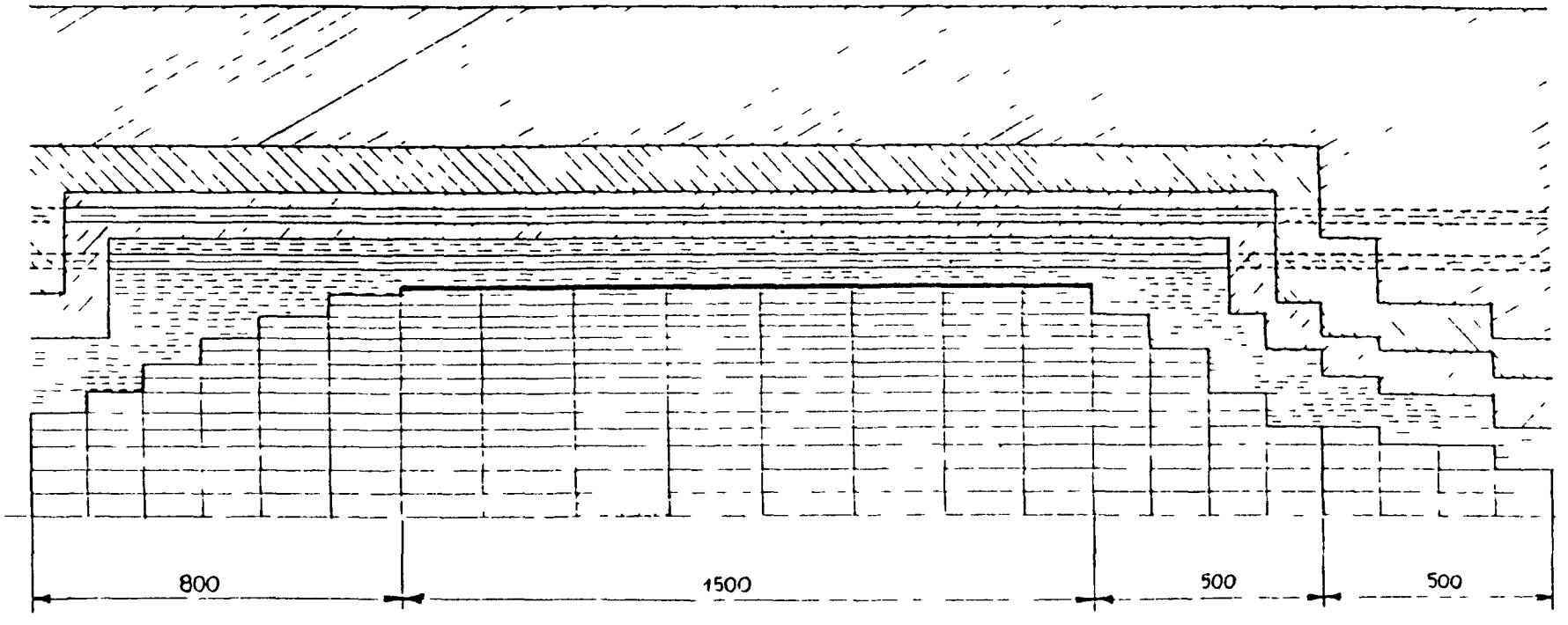

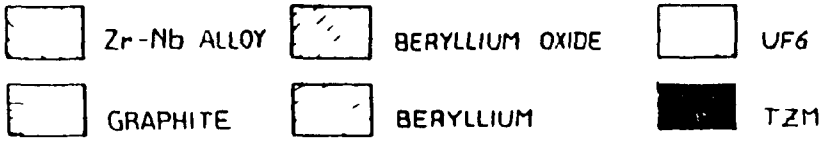

Fig. 3.2 Reactor model for nuclear analysis

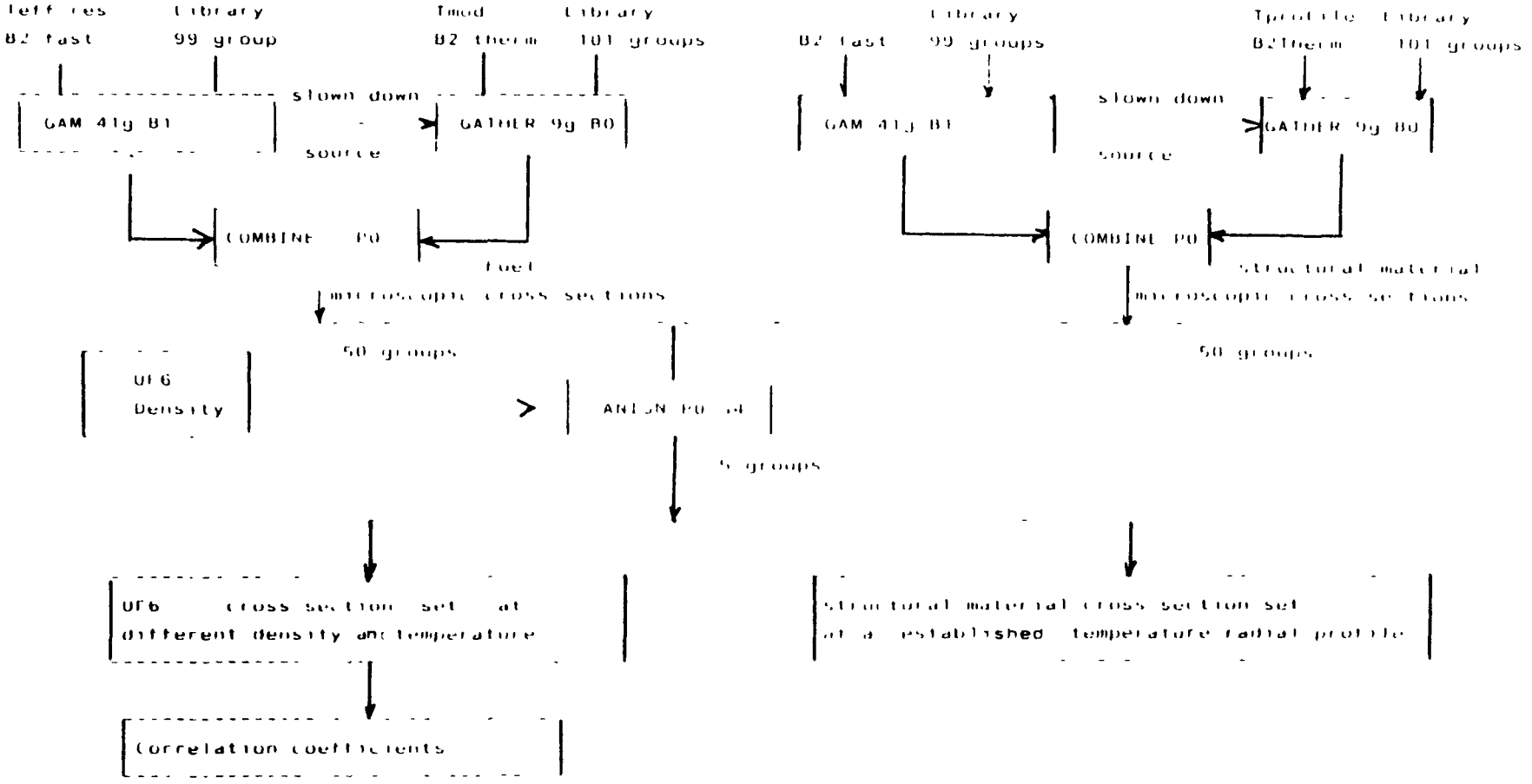

Fig 3 3 Macroscopic cross section generation

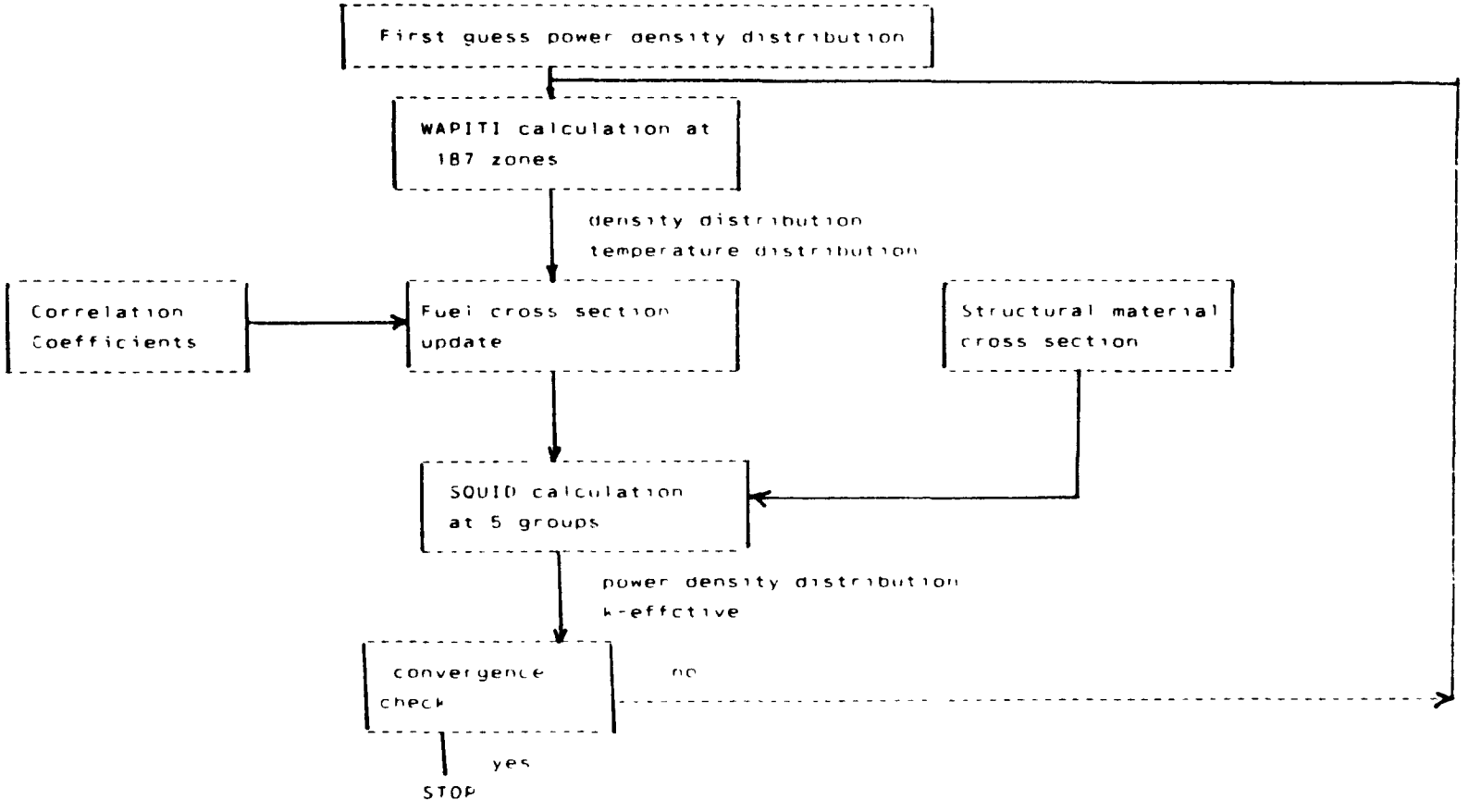

Fig.3.4 Flow chart for power density calculation

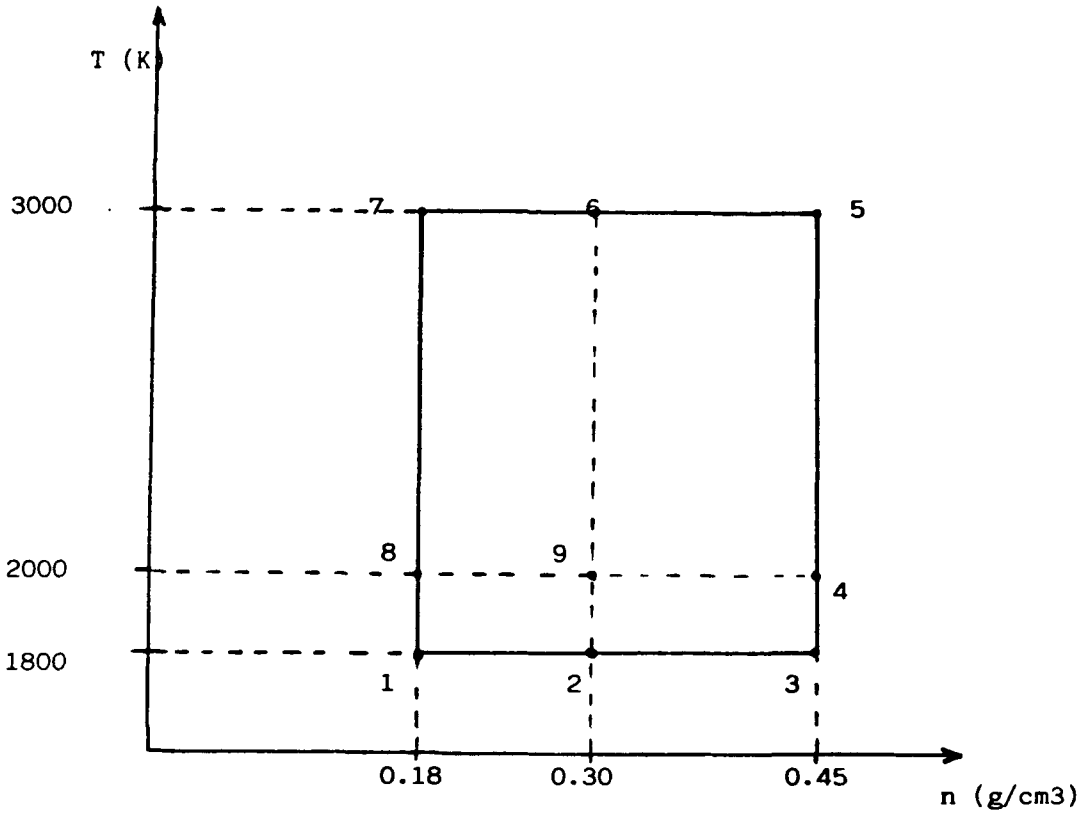

T: temperature
n: density

Fig. 3.5 Fuel characterization as a function of temperature and density.

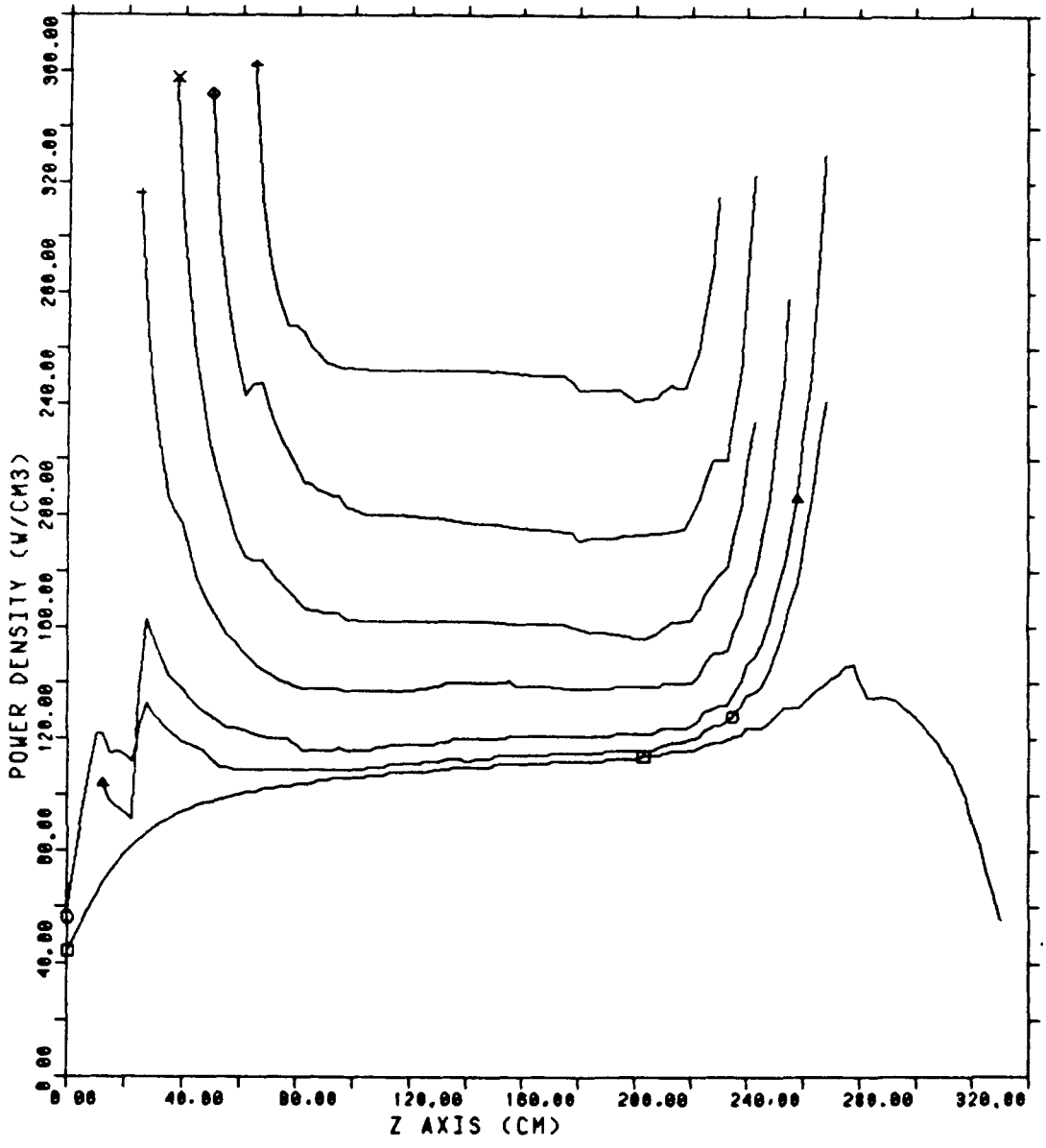

Fig 3.6 Power density vs. axial coord. (from core inlet) at different radial coordinates.
External reflector 100% in and 65% of the fuel through the annular diffuser.

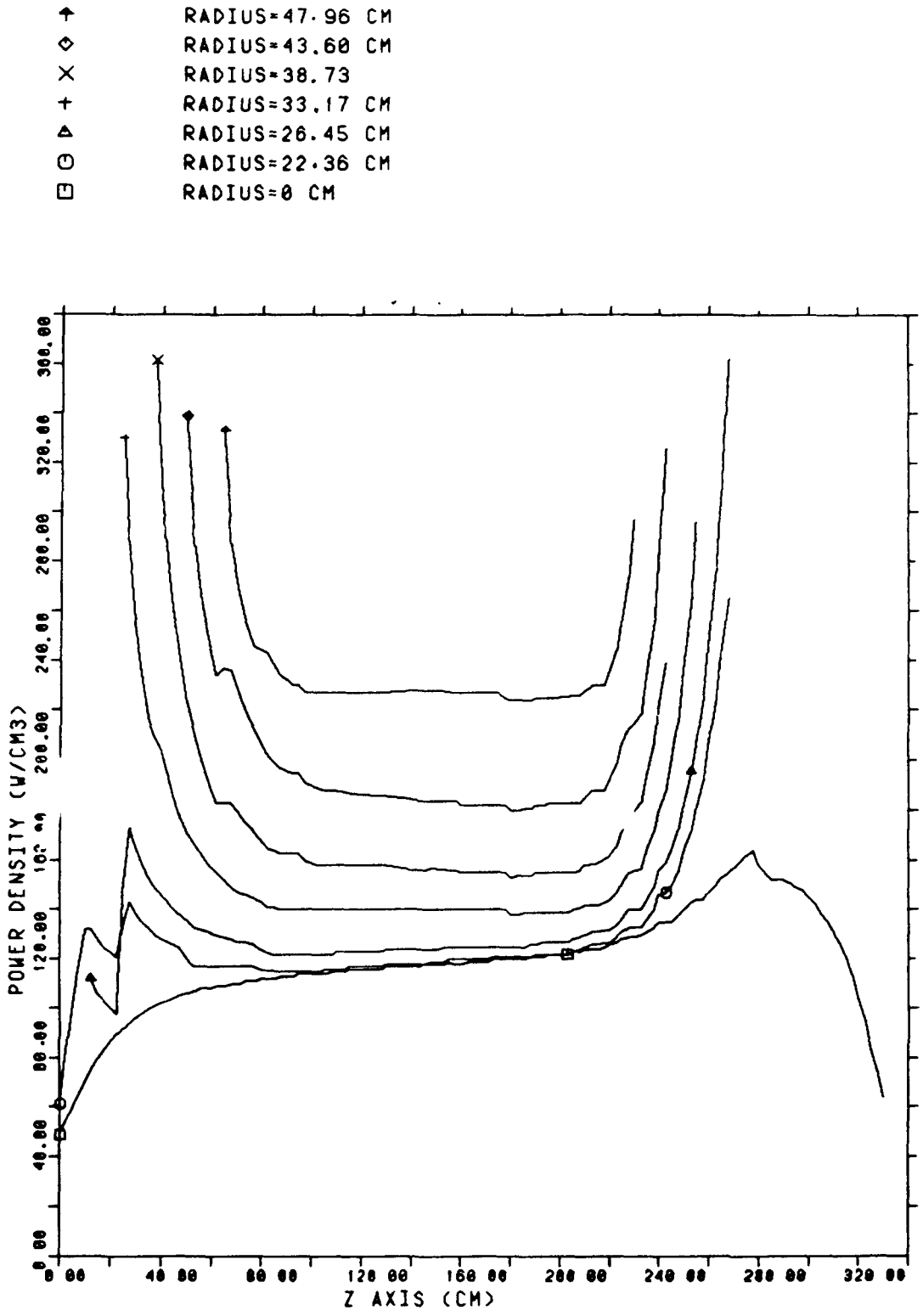

Fig. 3.7 Power density vs. axial coord. (from core inlet) at different radial coordinates.
External reflector out and 65% of the fuel through the annular diffuser.

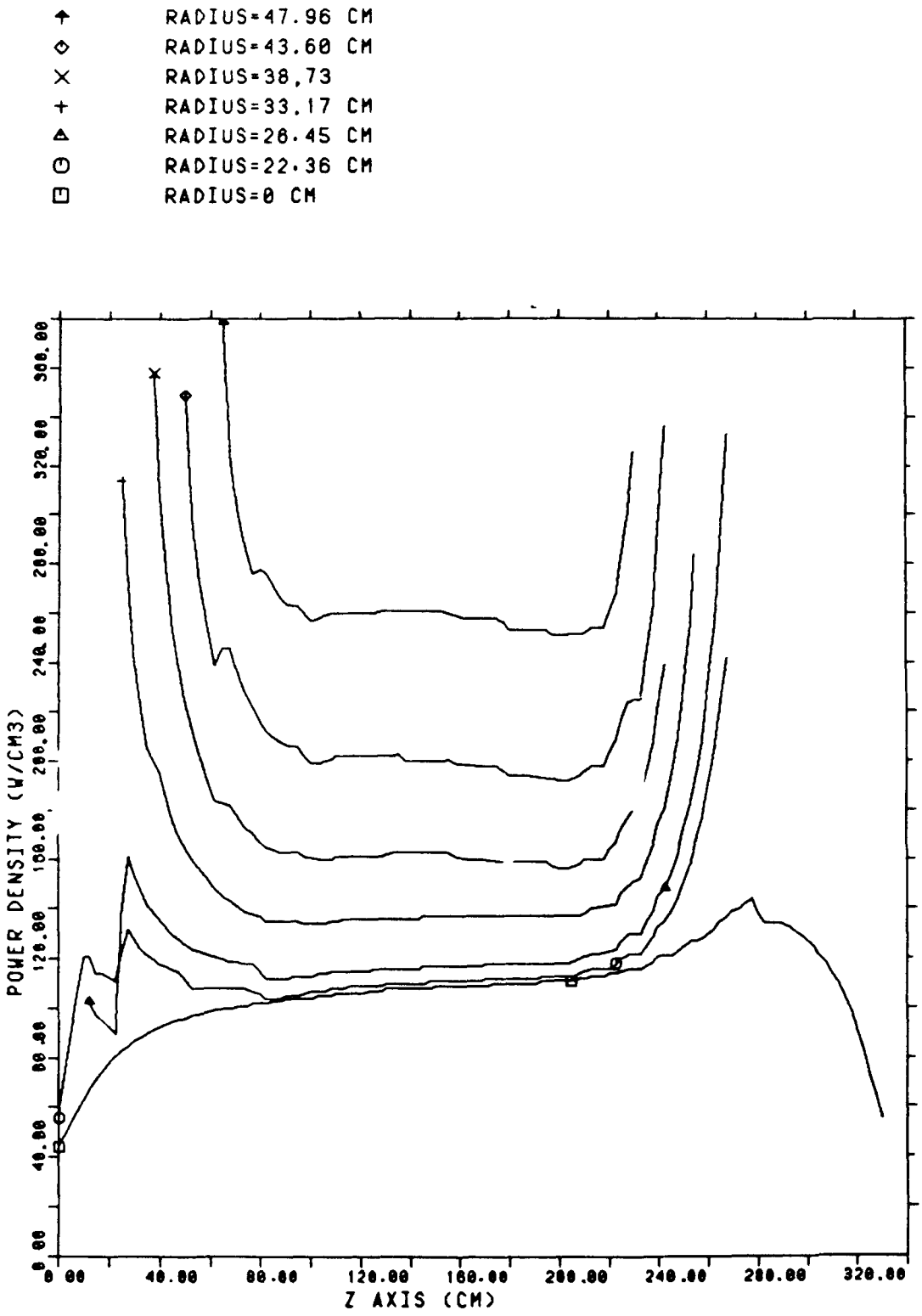

Fig. 3.8 Power density vs. axial coord. (from core inlet) at different radial coordinates.
External reflector 100% in and 70% of the fuel through the annular diffuser.

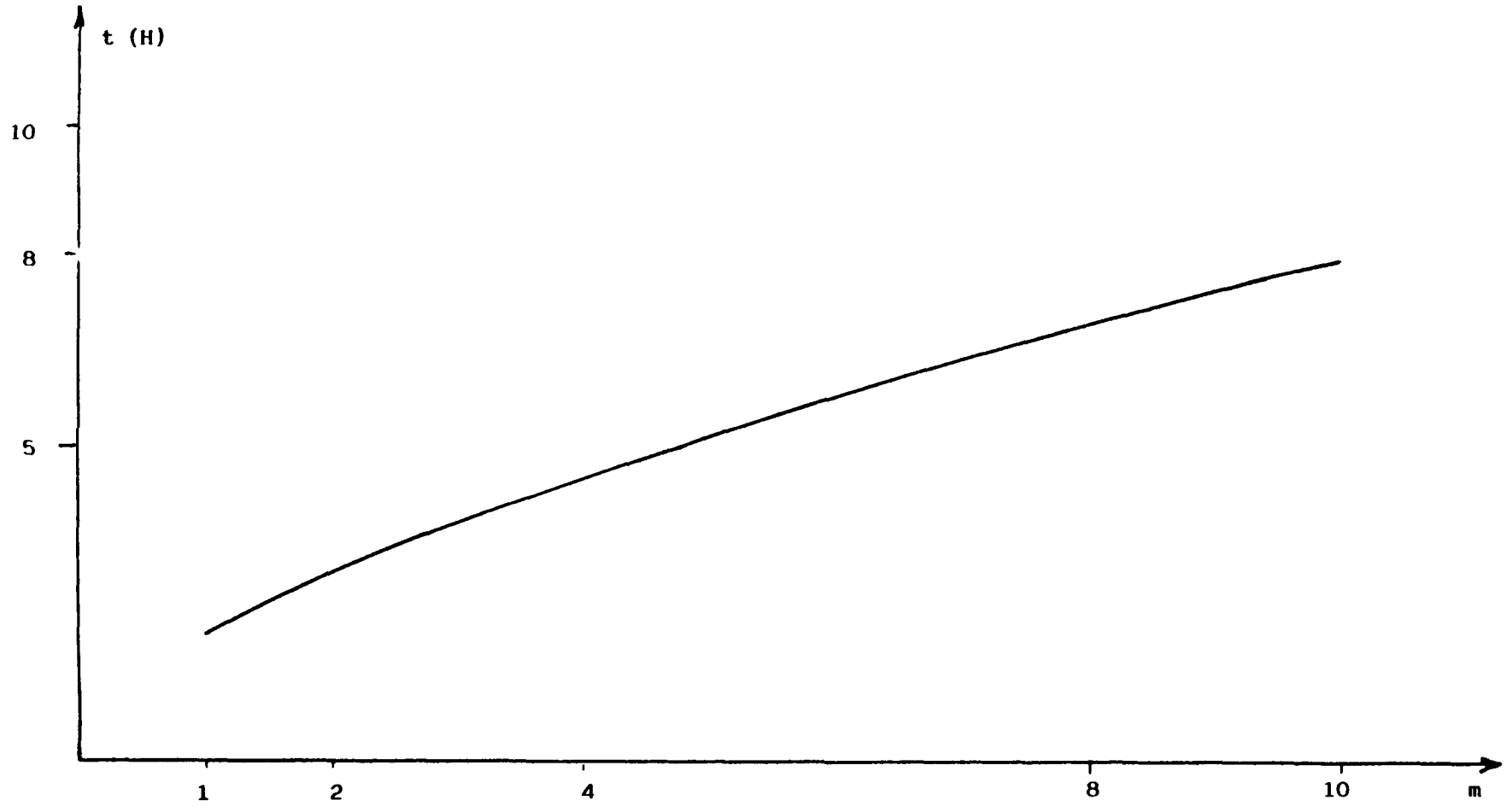

t: time

m: UF6 Overall Plant/Core Mass ratio

Fig. 3.9 Reactor life vs. UF6 Overall Plant/Core Mass ratio.
Reactor operated at full power level continuously.

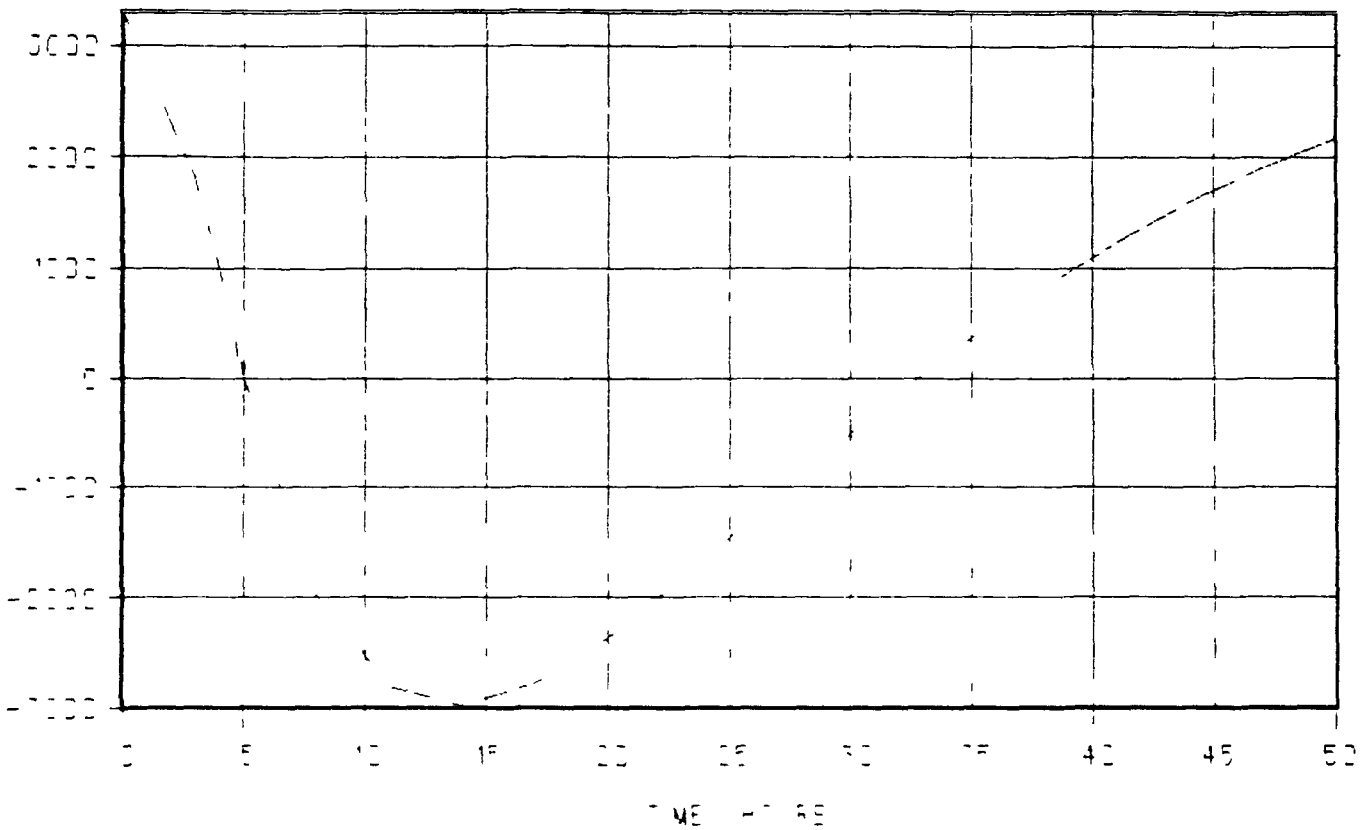

Fig. 3.10 Reactivity vs. time (UF6 mass ratio = 5).

4 WORKING FLUID CHARACTERISTICS

4.1 Symbols, Terms and Abbreviations

n	Number of particles per unit volume
Q	Collision cross section
v	Particle velocity
No	Number of neutral molecules per unit volume
α	Recombination coefficient
T	Temperature
ne	Number of electrons per unit volume
ni	Number of ions per unit volume
nc	Number of primary electrons per unit volume
τei	Thermalization time between electrons and ions
A	Quantity in the expression for thermalization time
k	Boltzmann s constant
m	Electron mass
A	Ion mass in amu
M	Ion mass
e	Electron charge
Γ	Quantity in the expression for coulomb collisions
eo	Energy of primary electrons
Tp	Temperature of primary electrons

T_s	Temperature of secondary electrons
T_i	Temperature of ions
τ_{ee}	Thermalization time between primary and secondary electrons
τ_{pei}	Thermalization time between primary electrons and ions
τ_{sei}	Thermalization time between secondary electrons and ions
I	Ionization potential
$\bar{R}$	Ionization degree
N_g	Number of gas molecules per unit volume
a,b	Coefficients in the rate equations
β	Ratio of n_0 to N_g
V_g	Gas velocity
x	Axial coordinate
	Average

4.2 Phase I

This phase provided a qualitative assessment of the types of primary reactions considered as the most important, and the evaluation of the relevant cross-sections, using current literature data and theoretical models.

The Production of Primary Electrons

Whenever 235U undergoes a fission reaction a number of ionizing agents are generated. Fission fragments are the most important as they absorb around 80% of the energy released. The energy balance of a fission reaction is illustrated in TABLE 1 (data are essentially similar for thermal or fast fission reactions and for the two uranium isotopes)[1].

TABLE 1

1.	Fission Fragments	165 MeV
2.	Prompt gamma rays (bremmstrahlung)	7 MeV
3.	Delayed gamma rays (discrete spectrum)	6 MeV
4.	ß+ and ß- rays	7 MeV
5.	Neutrons	5 MeV
6.	Neutrinos	10 MeV
TOTAL		200 MeV

Exceoting neutrinos, that are not stopped in the gas and escape from the core because of their extremely small cross-section, all the other remaining products are stopped within a few mms of gas (the neutrons travel the furthest distance but are, however, partly recovered by the reflector, and the gamma rays occur as electron-positron pairs in a few cms) and, therefore, they lose their energy partly by ionizing the constituent elements of the system and partly through the fission reactions.

In this phase we examined the elastic and inelastic cross-sections of the various fission products on gaseous UF6 and He [2]. Objective of the analysis was the evaluation of the number of ionizations that take place for each fission, neglecting the effects induced by this so called primary ionization.

The energy produced by the fission processes is largely converted into electrons;the majority of these (equivalent to about 165 MeV) are due to ionization processes induced by the fission fragments, and have a diffused spectrum with an average energy of 500 eV.

A smaller part (20 MeV) results from gamma ray conversion and beta decays and may have an energy of 1MeV per electron. However, in this case, the energy is rapidly distributed over other electrons, and hence it can be assumed, to a good approximation, that a single fission actually produces 4.10e5 primary electrons characterized by an average energy of 500 eV.

These primary ionizations are mostly made up by "stripping" an electron without modifying the molecular or atomic structure of the target.

4.3 Phase II

This phase addressed the study of the rate equations in the reactor core, providing an approximate analytical solution, and identifying the critical parameters.

The Production of Secondary Electrons

The primary electrons give rise to processes such as elastic and inelastic scattering (excitation of bonding electrons in the molecule), secondary ionization, and recombination.

Elastic scattering is low at energies greater than 10 eV and can be almost neglected in most cases. The inelastic scattering, on the other hand, is a very important reaction channel since it absorbs around 2/3 of the primary electron energy. This value is difficult to be computed or measured. It depends on the energy and on the structure of the molecules; data available in literature give a ratio between ionization and inelastic collision cross sections of 0.2 - 0.5 [3]. These reactions are part of the gas thermalization and heating process.

The atomic cross-section for ionization processes on UF_6 around 500 eV is of the order of 10e-15 cm^2. The cross-sections are known with errors of 25%. It should be noted that the ionization cross-sections on He have a very high threshold value, due to the high ionization potential (about 24 eV), and a very low value, due to the closed shell structure of He which permits elastic scattering to predominate. Hence, the addition of He is expected to increase the electrical conductivity to a very small extent.

The contribution to the ionization process is given by the product of the number of electrons, the cross-section, and the velocity. This yields, therefore:

$$dn/dt = +nQ\langle v\rangle Ng$$

where Q is the cross section, numerically equal to 10e-15, $\langle v\rangle$ is the velocity in cm/sec. equal to $\langle v\rangle = 6.10e7\sqrt{T}$ (where T is the temperature given in eV) and Ng is the number of molecules per cm^3.

The probability of ionization by collision should be actually obtained by averaging the cross-section, which depends upon the electronic energy, over the assumed Maxwell velocity distribution [4]. However, the numerical value indicated for Q is correct for the order-of-magnitude estimate of this phase.

Recombination

The neutralization probability of the ionized system is related to the product of the electronic density, the ionic density, and the density of a third element essential for energy and momentum conservation [4]. This third element may be either a neutral atom or an ion, or even an electron. The higher mobility of the electrons makes the following the preferred recombination process in our case :

$$n_e + n_e + n_i \rightarrow n_e + n_i$$

This parameter is extremely sensitive to the density and temperature of the system.

The rate of recombination can be expressed by the following relation:

$$dn/dt = - \alpha n^2$$

where $\alpha = 10e-25n/T^{4.5}$, n is the electron (or ion) density per cm^3 and T is the temperature expressed in eV.

Note the dependence upon n^2 (the coefficient α is linearly related to n), which reminds that recombination is a three-body process [5].

The dependence on T is very strong because the electron velocity is the other key parameter to the problem, both when calculating the cross-section and when successively calculating the average on the velocity distribution, necessary to determine the probability per second of the process.

Simplified Rate Equation

The effects of recombination and ionization may be combined into a rate equation for the electronic part of the system:

$$dn/dt = n\Omega\, v\, Ng - \alpha n^2$$

Substituting the numerical values into the above equation yields:

$$dn/dt = n\ 3.10e13\ T\sqrt{T} - 10e{-}25\ n^3/T^{4.5}$$

Ng was assumed to be 5.10e20 molecules per cm^3.

Let us now suppose to be under steady state conditions (hence neglecting dn/dt).

This assumption requires that a unique equilibrium temperature exists, at least among the various ionized species, and that the time to reach such conditions is much shorter than the time during which the gas remains in the reactor core. In fact,

electrons around 500 eV, electrons of a few eVs (secondary), and ions at almost the same temperature of the gas coexist during a first phase.

However, as we shall see better afterwards, the conditions in the reactor core lead to extremely short thermalization times compared with the transit time of the gas, and hence, in spite of the simple approach, this first evaluation may be considered quite realistic.

Let us now introduce the energy balance, that is determined by the distribution of the ionization and thermalization energies:

$$y n_0 500 = n(T+I) = n(T+10) = y 2.8 \cdot 10^{21}$$

where $y<1$ is the part of energy involved in ionization processes and I is assumed to be equal to 10 eV, a value typical of most atoms and molecules.

The rate equation, once inserted into the balance equation, gives:

$$T^{3/2} \cdot (T+10) = 165y \Rightarrow T \cong 2.8y^{2/3}$$

Similarly, the implicit value of the electronic density can be found:

$$n = 6 \cdot 10^{5} (2.8 \cdot 10^{20} y - n)^{3/2}$$

which yields approximately

$$n = 2.8 \cdot 10e20y$$

It should be noted that the recombination process is active, above all, at low temperatures. However, the process temperature is determined critically through the parameter y. The conventional thermal region (T 4000 C) is indicated by values of y less than 10e-2.
Therefore, the critical parameter that must be calculated is the actual distribution of energy between the ionization and thermalization processes or, if one prefers, the electron equilibrium temperature.

Thermalization Times

What remains to be seen is whether the secondary electrons, which still have sufficiently high energy, of the order of 2-3 eV, can thermalize (and hence recombine) rapidly or not.
The electron-ion thermalization time decreases with the temperature according to the following relationship [5]:

$$\tau_{ei} = \frac{\theta}{n} (kT)^{3/2}$$

where θ is given by [5] as:

$$\theta = \frac{3\, m^{1/2}\, 1836\, A}{8(2\pi)^{1/2}\, e^4 \log\Gamma}$$

where m is the electron mass, e the electron charge, A the ion mass in a.m.u., and $\log\Gamma$ a parameter which varies slightly with density and temperature (it is related to the smallest collision parameter in a Coulomb interaction). In the case of UF6, the value of θ is 3.10e9, with kT expressed in eV. Assuming that the final energy has a value of a few eVs, with a density of about 10e19 el/cm^3, the electron-ion thermalization time is of the order of 10e-9 s.

Another important parameter is the electron-electron thermalization rate. In fact, in our case, high energy electrons (around 500 eV) and secondary electrons (around 10 eV) will coexist for a certain period of time. The electron-electron thermalization time is reduced by the electron/ion mass ratio, that is $\tau_{ee}=(1/1836A)\tau_{ei}$. Both thermalization times are much shorter than the gas replacement time (0.1 s, typically) and, hence, it is reasonable to assume steady state conditions to calculate the concentrations of the chemical species in the reactor.

Complete Rate Equations

The "complete" rate equations take actually into account only a few of the numerous possible reactions in the system. On the basis of the cross-section experimental data and of the analysis reported in the previous paragraphs, we selected the reactions which were considered as the most significant for the purpose of this study.

reactions such as the multiple ionization of atoms or molecules have been neglected. In other words, only UF_i, UF_i^+ (with i=0,6) and F^- type systems are considered and possible states such as UF_i^-, UF_i^{++}, etc. are neglected.

Under this assumption, there are 18 unknown parameters in the problem:

$n_i = UF_i/cm^3$ (7 variables),

$n_i^+ = UF_i^+/cm^3$ (7 variables),

$n_f = F/cm^3$,

$n_{f2} = F_2/cm^3$,

$n_{f-} = F^-/cm^3$ (3 variables),

in addition to n that represents, as before, the number of free electrons. Therefore 18 equations are required to solve the system as a function of three basic input parameters: Ng (gas density in the reactor), no (number of primary electrons) and the average primary radiation energy eo = 500 eV.

The rate equations provide 17 relations, one for each variable: the energy balance yields the missing condition (system neutrality is implicit in the rate equations).

Method of Solution

Before proceeding, it is necessary to discuss some assumptions that should be introduced in a numerical approach to the evaluation of ionization levels and gas composition in the cavity.

1) The system is homogeneous.

This is a good approximation given the parameters of the reactor and the properties of the system being examined. In fact, the mass transfer rates are very small in comparison with two significant fluid parameters, the thermal transfer rate and the speed of sound; in addition, the thermalization processes take place on small space scales, of the order of a few cms. Hence, there is no use in introducing the convection terms into the rate equations, and considering the unknowns as a function of position.

2) The system is under steady state conditions.

This assumption is undoubtedly true when considering the thermalization time scale (10e-9 s), and allows the rate equations to be simplified considerably by neglecting the time dependence of the variables.

3) Cross-section values.

In our approach, there are 46 cross-sections (which are strongly energy dependent) constituting a set of input parameters to the problem. They are not variables but physical quantities that can be experimentally measured. In any case, these parameters are not

well known and it is therefore necessary to create a simple theoretical model to predict the cross-section relative weights and their dependence on energy.

The system can be solved by means of successive iterations. A tentative value is assumed for the number of electrons (for example the value calculated with the simplified equation shown previously) and the system solved with this value. The solution in this case is very simple because the system is almost linear since the majority of the quadratic functions are related to the presence of the unknown n. Now the average energy is calculated, the values of the cross-sections are redefined and the number of electrons recalculated using the first rate equation. The value thus obtained is inserted back into the equations and the procedure repeated. After a few iterations the result begins to converge towards the exact value.

4.4 Phase III

This phase addressed the study of the rate equations in the MHD channel, providing a simplified set of equations for numerical solution.

The following assumptions have been introduced to describe the evolution of ionization degree and temperature in the MHD channel:

1) gas density is uniform during the transit time in the channel;

2) a uniform distribution of fission reactions provides a uniform background of primary electrons (500 eV);

3) as a first approach, the secondary species are supposed to derive essentially from the ionization of UF6. Therefore, the maximum level of charge density cannot overcome gas density. The consequences of this statement will be discussed later;

4) the loss of electrons is ascribed to three-body recombination;

5) since the local neutrality condition is well verified because of the very short Debye length compared with plasma dimensions, it is assumed ne=ni for secondary charges.

Even a simplified approach requires to solve the system giving the thermal exchange rates among the ionized species. Since charge density is variable, the energy balance must be coupled to the rate equation for electron production:

$$n_o \frac{dT_p}{dt} = - \frac{n_o T_p - n_e T_s}{\tau_{ee}} - \frac{n_o T_p - n_e T_i}{\tau_{pei}} \qquad (1)$$

$$n_e \frac{dT_s}{dt} = \frac{n_o T_p - n_e T_s}{\tau_{ee}} - \frac{n_e T_s - n_e T_i}{\tau_{sei}} \qquad (2)$$

$$n_e \frac{dT_i}{dt} = \frac{n_o T_p - n_e T_i}{\tau_{pei}} + \frac{n_e T_s - n_e T_i}{\tau_{sei}} \qquad (3)$$

$$\frac{dn_e}{dt} = \frac{a}{I} N_o \left(\frac{\exp(-I/T_p)}{T_p^{1/2}} n_o + \frac{\exp(-I/T_s)}{T_s^{1/2}} n_e \right) - n_e \tau_s \qquad (4)$$

Equations (1), (2) and (3) represent the cooling of primary electrons by thermal exchange with secondary electrons and ions, the heating of secondary electrons by exchange with the primary ones and the transfer of energy from secondary electrons to ions (Eq.(2)), and finally the heating of ions. T_p, T_s and T_i are the temperatures (in eV) of primary electrons, secondary electrons, and ions, respectively. n_o is the uniform and constant density of 500 eV electrons, $n_e = n_i$ is the charge density produced by additional ionization.

τ_{pei}, τ_{sei}, and τ_{ee} represent the thermalization time constants for the involved interactions. The general form of τ has been given in the previous paragraph. Therefore, the time constants of Equations (1), (2) and (3) are given by:

$$\tau_{ee} = \frac{\theta}{n_e} (kT_p)^{3/2} \quad \text{and} \quad \tau_{pei} = 1832 \tau_{ee}$$

$$\tau_{sei} = 1832A \frac{\theta}{ne} (kT_s)^{3/2}$$

In Eq.(4), the first term represents the rate of ionization produced by primary and secondary electrons, and the second one the three-body recombination of secondary charges, the fissions providing the gas with a continuos source of primary electrons.

I is the ionization potential, a and b are numerical coefficients, and No is the density of neutral molecules, related to ne by the mass conservation relation.

It is useful to introduce the degree of ionization as a variable, namely R=ne/Ng where Ng is the gas density. The density of neutral molecules is replaced by No=Ng-ne, and the density of primary electrons by no=ßNg: no is given by the number of fissions/cm³s times the ionization efficiency of each fission, whose value has been estimated in a previous paragraph at about 4.10e5. Therefore, the system of Equations (1)-(4) is transformed in

$$\frac{dT_p}{dt} = -\frac{RN_g}{\theta T_p^{3/2}} \left[T_p - \frac{R}{\beta} T_s - \frac{m}{M}\left(\frac{T_p}{T_s}\right)^{3/2} (T_s - T_1) \frac{R}{\beta}\right] \qquad (5)$$

$$\frac{dT_s}{dt} = \frac{\beta N_g}{\theta T_p^{3/2}} \left[T_p - \frac{R}{\beta} T_s - \frac{m}{M}\left(\frac{T_p}{T_s}\right)^{3/2} (T_s - T_1) \frac{R}{\beta}\right] \qquad (6)$$

$$\frac{dT_1}{dt} = \frac{m}{M}\,\frac{\beta N_g}{\theta T_p^{3/2}}\left[T_p - \frac{R}{\beta}\,T_s - \frac{m}{M}\left(\frac{T_p}{T_s}\right)^{3/2}(T_s - T_1)\frac{R}{\beta}\right] \qquad (7)$$

$$\frac{dR}{dt} = \frac{aN_g(1-R)}{I}\left[\frac{\exp(-I/T_p)}{T_p^{1/2}}\,\beta + \frac{\exp(-I/T_s)}{T_s^{1/2}}\,R\right] - \frac{bN_g^2R^2}{T_s^{1/2}} \qquad (8)$$

The assumption of a uniform density distribution, related to the rather flat profile of gas density during the transit in the channel, allows one to neglect the contribution of the terms $V_g.\mathrm{grad}(T)$ and $V_g.\mathrm{grad}(n)$ in comparison with the time derivatives. Therefore, an elementary volume of fluid is modified in its properties before appreciable displacement takes place. As a consequence, the integration in time is equivalent to follow the space evolution, with the variable change $x=V_g.t$. It turns out that a non-uniform source of primary electrons can be included in the model, under the condition that the induced gradients still verify the inequality $V_g.\mathrm{grad}(T) \ll dT/dt$ and $V_g.\mathrm{grad}(n) \ll dn/dt$. For instance, in the presence of a step distribution of the fission source in a length x_0, it is sufficient to introduce, in the solution of the system, the condition $n_0=0$ for $t>x_0/V_g$. Alternatively, the system can be solved in the space variable by introducing $dx=V_g.dt$. In general, it is not strictly

required that gas velocity and density are uniform and constant; it is sufficient that significant variations of Vg and density occur in a time longer than the time required to reach a stationary state for Tp, Ts, Ti, and R.

4.5 References

[1] Gladstone, "Nuclear Reactor Theory", Pergamon Press, 1964.

[2] Ziegler J.F., "Stopping Power and Ranges in Elemental Matter", Pergamon Press, 1977 - 1981.

[3] Golant V.E., Zilinskij A.P., Sacharov I.E., "Osnovy fiziki plasmy" ("Fundamentals of Plasma Physics"), MIR, Moscow, It. transl. 1983.

[4] Zeldovich and Raizer, "Physics of Shock Wave and High Temperature Hydrodynamic Phenomena", Academic Press, New York, 1966.

[5] Spitzer L., "Physics of Fully Ionized Gases", Interscience, New York, 1956.

5 ELECTRICAL CONDUCTIVITY EFFECTS

5.1 Symbols, Terms and Abbreviations

σ	Electrical conductivity
Mc	Mass of the superconducting coil
Pg	Power generated by the MHD channel
ρc	Conductor mean density
μo	Fermeability of free space
J	Current density
L	Channel length
D	Channel diameter
u	Gas velocity
B	Magnetic field strength
Ms	Mass of the magnet structure
ρ	Density of the structural material
st	Working stress level of the structural material
T1	Gas temperature at the compressor inlet
Ø	Neutron flux along the duct
Øo	Neutron flux at the entrance of the duct
d	Diameter of the entrance section of the duct
x	Axial coordinate along the duct
Ue	Electron velocity
Ui	Ion velocity
E	Total electric field

E_o	External electric field
E_{int}	Internal electric field
e	Electron charge
m	Electron mass
M	Ion mass
ν_{et}	Total collision frequency for electrons
ν_{it}	Total collision frequency for ions
k	Boltzmann's constant
T_e	Electron temperature
T_i	Ion temperature
n_e	Number of electrons per unit volume
n_i	Number of ions per unit volume
n	Number of particles per unit volume
Q	Collision cross section
N_g	Number of gas molecules per unit volume
R	Ionization degree
θ	Quantity in the expression for thermalization time
D_i	Diffusion coefficient of electrons
D_e	Diffusion coefficient of ions
μ_e	Electron mobility
μ_i	Ion mobility
T_s	Temperature of secondary electrons
c	Coefficient in the conductivity relation
Q_N	Collision cross section with neutrals
T_p	Temperature of primary electrons

T_i	Temperature of ions
a,b	Coefficients in the rate equations
no	Number of primary electrons per unit volume
β	Ratio of no to Ng
$\bar{\xi}$	Number of primary electrons per fission
nf	Number of fissions per unit volume
t	Time
τ	Time constant
I^-	Attachment energy
a^-	Coefficient in the attachment equation

5.2 Channel Characteristics and Conductivity

To proceed further in the analysis, it is necessary to combine conductivity calculations with actual channel (and nozzle) characteristics. In fact, the results of the former depend directly on the latter, as channel and nozzle lengths, along with the density distribution of the gas flowing through them, are required to solve the rate equations (1)-(4) or (5)-(8) given in section 4.4. Furthermore, the same characteristics influence the distributions of residual fission neutrons and gamma rays available in the duct which, in turn, provide the source of primary electrons to be introduced in the rate equations. On the other hand, the channel operating characteristics are largely dependent on the conductivity levels assumed in the analysis. For this reason, a parametric approach has been adopted, and the generator performance has been estimated for two levels of conductivity, namely $\sigma=10$ and $\sigma=100$ $(\Omega m)^{-1}$. The nozzle and channel configurations arising from this process have been tested to verify if they were consistent with the conductivity levels resulting from the rate equations. Channel performance has been evaluated under the following assumptions:

- Faraday configuration of the generator electrodes with a load factor of 0.9;
- Straight channel with a constant aperture angle of 7°;
- Nozzle inlet temperature and pressure of 2300 K and 15 MPa, respectively;

- Channel flow rate of 1000 kg/s:

A 1-D thermal-fluid model of the channel and nozzle ducts has been adopted in the analysis. For each of the two reference levels of conductivity, a number of channel configurations have been compared as a first approach by using the specific mass relation given by Rosa in [1] for a channel of length L and diameter D:

$$\frac{M_c}{P_g} = \frac{16}{\mu_0}\left(\frac{\rho_c}{J}\right)\left(\frac{L}{D}\right)\left(\frac{1}{P_g}\right)^{1/2}\left(\frac{1}{\pi\sigma u^2 B^{1/2}}\right)^{2/3} \qquad (1)$$

where ρ_c is the conductor mean density and J is the current density. This relation gives the mass of a superconducting coil per unit of generated power. In the conditions of the analysis, the mass of the structure required to hold the coil together should be comparable with the coil mass given by Eq. (1). A lower limit for the former can be estimated with the following relation:

$$M_s = \frac{\rho}{stJ}\int \frac{B^2}{\mu_0}\,dv \qquad (2)$$

where ρ is the density and st is the working stress level of the structural material. This relation too is derived from [1]; the structure unit mass for a saddle coil is expected to be within a factor 2 of the value given by Eq. (2).

In addition to the two levels of conductivity mentioned above, the configurations that have been investigated are featured by different values of the inlet Mach number and induction field of the generator duct. The parameters assumed in the analysis enable to extract power in the 120-150 MWe range, limiting the induction field strength at reasonable values (6 T at most), observing the constraints on the length to diameter ratio imposed by heat and pressure losses, and obtaining a specific mass (from Eq. (1)) in the range of 10e-2-10e-3 kg/kWe. This range is in the reach of both reference levels of conductivity; however, a decrease of σ must be offset by a corresponding variation of other terms in Eq. (1). In particular, the values of u and B are assumed as independent parameters, while L/D and Fg are derived from the calculations. It is evident that a higher level of conductivity makes it possible to attain the desired range of power density with lower values of B and, especially, of u (and, hence, of the Mach number at the generator inlet). This latter condition appears to be of special importance, as a lower gas velocity in the channel means a shorter nozzle before the channel. On the other hand, the distance between the generator and the reactor cavity has a strong influence on the actual level of conductivity. The results show that, if one pursues a high power

density condition (that is, essentially, a high value of σu^2), the system should work at a high conductivity, low velocity condition, rather than the opposite.

It should be pointed out that such influence is not connected with the effect of the field on the reactor core, which is negligible, due to the different order of magnitude of the fission ion gyro radius in comparison with their mean free path. In fact, the nozzle length turns out to be of critical importance because of the sharp decrease of residual fission and gamma densities as a function of the distance from the reactor outlet.

Finally, a few considerations about the parameters adopted in the analysis.

The value of nozzle inlet temperature (2300 K) has been partly assumed on the basis of material requirements, by analogy with conventional MHD converters, and partly to maintain an adequate level of cycle efficiency with a high heat rejection temperature (T1=600-900 K, T1 being the compressor inlet temperature), as a space-based system is expected to require. Within this range of T1 and with the other cycle parameters indicated in this section, efficiency may vary between 0.12 and 0.36. It should be stressed that cycle efficiency is heavily influenced by heat rejection temperature and regenerator performance; both characteristics should be ultimately selected on the basis of minimum system mass, rather than maximum efficiency.

The nozzle inlet pressure (15 MPa) is equal to the average operating pressure of the reactor, which was derived on the basis of an average reactor temperature and density of 2000 K and 0.3 g/cm^3, respectively. The latter is the result of a preliminary estimate of criticity. The same calculations gave the cavity diameter (1 m) assumed in the neutron analysis.

The flow rate of 1000 kg/s results from the power output to be generated by the converter, assumed in the range 120-150 MWe gross and 20-30 MWe net. The latter is actually a lower limit applicable to the highest rejection temperature assumed in the calculations: the net output increases to 60-80 MW when T1 is lowered to 600 K.

The temperature of the gas at the reactor inlet (1770 K) has been obtained through a preliminary analysis of the working cycle, and it is typical of regenerative Brayton cycles operating between the temperature levels mentioned above. The same analysis gave the reference value of 277 MW for the thermal power provided by the reactor.

5.3 Fission and Gamma Density in the Channel

The fission and gamma power densities in the MHD expansion channel must be estimated to solve the rate equations and evaluate the conductivity levels.

Fission Power Density

The fission power density calculations have been carried out by means of the following approximations:

1. Preliminary evaluation with a simplified method (see Ref. [2], pag. 290).
2. SOLID- 360 [3] diffusion calculations with a simplified two-dimensional R-Z geometry and walls fabricated from Al2O3 or BeO.

In order to estimate the power density, the duct has been divided into a finite number of regions with different UF6 density (see Fig. 5.1 and Fig. 5.2).

For each region, the fission macroscopic cross sections have been derived from the core cross sections calculated during Task 1, reduced by the appropriate density factors.

The neutron flux level inside the MHD channel has been calculated as transmission through a cylindrical duct.

Preliminary evaluation. The neutron fluxes at the inlet of the nozzle have been derived from the nuclear analysis of Task 1.

The effect of wall material reflections and working fluid absorptions have been neglected.

The uncollided fluxes along the duct have been calculated with the formula:

$$\phi = \phi_0 \frac{d^2}{8x^2}$$

where Øo is the flux at the entrance of the nozzle, d is the diameter of the entrance section of the nozzle, and L is the distance between the entrance of the nozzle and the point where the flux is calculated.

The results (MeV/cm²s) are reported in Tab. 5.1.

Diffusion Calculations. In order to estimate the influence of wall material and thickness on fission power density, a second analysis of the MHD channel has been carried out by the SQUID-360 diffusion code, using the R-Z geometry to model the Power Conversion Unit (gas reactor + nozzle and MHD channel), and the cross sections derived from Task 1..

The configuration extends radially to include the movable reflector and axially from the core midplane to 1200 cm in the channel (see Fig. 5.2).

As to the spatial discretization, 114 axial and 37 radial meshes have been used.

The duct has been divided into 9 regions with different UF6 densities carried out from Fig. 5.3.

The nozzle and channel walls have been assumed to be fabricated from Al2O3 or BeO. For each material, two values of wall thickness have been examined: 3 cm and 6 cm. The adoption of a two-dimensional model doesn't account for the presence of the electrodes. However, it shouldn't be unreasonable to assume an electrode wall consisting of "thin" electrodes mounted on "thick" insulating blocks; furthermore, the electrodes themselves might

be fabricated from zirconia based materials, and zirconium possesses favourable properties being a low capture cross-section material, which would allow to exploit the potential of a moderating layer.

As previously mentioned, the calculations have been carried out by using the cross section data from Task 1. collapsed to a 5 group structure.

The fission power for each region is shown in Fig. 5.4. The results of the cases examined are reported in Tab. 5.2.

Gamma Power Density

The gamma fluxes in the MHD channel have been calculated by the MERCURE IV point kernel code [4].

The gamma source, consisting of fission gamma, is located in the core.

Build-up factors have been used in the MERCURE calculation.

The geometry of the analyzed configuration is shown in Fig. 5.1.

The core has been divided into 3 regions and the duct into 6 regions with different UF6 density.

Region-wise UF6 densities in the duct have been carried out from Fig. 5.3.

The nozzle and channel walls are assumed to be fabricated from Al2O3 material, but they have not been taken into account for streaming calculations.

The calculations have been performed by using the BIF 62 library cross section data from Ref. [5].

The results are reported in Table 5.3.

5.4 Conductivity Calculations

A Relation for Conductivity

Owing to the range of gas transit time in the channel (≈ 10 ms) and to the very small Debye length compared with the dimensions of plasma, the motion of both charged species can be described by neglecting the convective derivatives of the velocities and assuming the neutrality condition ne=ni. Therefore, the velocities Ue and Ui are given by [6]

$$U_e = -\frac{eE}{mV_{et}} - \frac{kT_e}{mV_{et}}\frac{\mathrm{grad}(n)}{n} \qquad (1)$$

$$U_i = \frac{eE}{MV_{it}} - \frac{kT_i}{MV_{it}}\frac{\mathrm{grad}(n)}{n} \qquad (2)$$

where E represents the total electric field, given by the superposition of an external field Eo and the internal field Eint generated by the relative motion of charges. V_{jt} is the total collision frequency including momentum-exchange collisions with neutrals and between electrons and ions, namely

$$V_{jt} = \langle Q U_j \rangle N_g (1-R) + \frac{R N_g}{\theta T_e^2 \tau} \qquad (3)$$

where the symbols have been previously defined. The internal field is obtained by equating the fluxes of ions and electrons, in accordance with the neutrality condition. It turns out that in the absence of an external field, the current is zero. The internal field is given by

$$E_{int} = \frac{D_i - D_e}{\mu_e + \mu_i} \frac{\mathrm{grad}(n)}{n}$$

where $D_j = kT_j/m_j V_{jt}$ is the diffusion coefficient and $\mu_j = e/m_j V_{jt}$ is the mobility. Therefore, current density becomes

$$J = en(U_i - U_e) = e^2 n(\mu_e + \mu_i) E_o = \frac{e^2 n}{m V_{et}} E_o \qquad (4)$$

where the mobility of ions has been neglected, because of the very small mass ratio. By using the same notations, the conductivity is given by

$$\sigma = \frac{e^2 R T_s^{3/2}}{m[cT_s^2(1-R)+R/\theta]} \qquad (5)$$

where Ts is in eV and c is proportional to the cross section with neutrals. In MKS units

$$\sigma \approx \frac{10e-2RT_s^{3/2}}{3.10e7QNT_s^2(1-R)+10e-4R} \quad (\Omega m)^{-1} \qquad (6)$$

QN is the geometrical cross section with neutrals in cm^2. If the contribution of collisions with neutrals is negligible, the conductivity is independent on the degree of ionization R and increases as Ts increases. With a typical value of QN≈10e-15, the conductivity is only function of Ts if the condition

$$R \gg \frac{3.10e-4T_s^2}{1+3.10e-4T_s^2}$$

is verified. In case of total ionization (R=1), the conductivity is simply equal to $10e2Ts^{3/2}$. If Ts≈10 eV, a degree of ionization of 10% is sufficient to give $\sigma=3.10e3\ (\Omega m)^{-1}$.

Numerical Results and Discussion

The system of Equations (5)-(8) derived in section 4.4 has been solved by the Runge-Kutta fourth order method. The initial conditions are Tp=500 eV, Ts=1 eV, Ti=0.5 eV and R=0. They correspond to typical mean values; however, the stationary values don t depend on the initial conditions. The a and b parameters in Eq.(8) are chosen on the basis of data available in literature, namely a=10e-6 and b=10e-22 (cgs units). The value of b is probably more realistic than that given previously; in any case, an overestimation of the recombination rate gives the lowest limit of achievable ionization. The ionization potenzial of UF6 is ≈15 eV. The thermalization coefficient is 10e4 (cgs units). The initial rate of primary electrons β is related to the number of fissions i.e $\beta=\xi nf/Ng$, where ξ represents the number of 500 eV electrons per fission, whose value has been estimated at 4.10e5. Figures 5.5-5.7 show the time evolution of temperatures and degree of ionization at different initial gas densities. It has been assumed β=10e-2, that corresponds to nf=2.5e10-8Ng.

Under the conditions of Fig.5.5 (Ng=5.10e17 molecules/cm^3), the system reaches a stationary configuration in less than 1 μs, with Tp=24 eV, Ts=T1=3.7 eV and R=0.067. The resulting conductivity is σ=7.10e2 $(\Omega m)^{-1}$.

Figures 5.6 and 5.7 show the system evolution with Ng=3.10e18 molecules/cm^3 and Ng=10e20 molecules/cm^3.

The stationary data referring to Fig. 5.6. are Tp=140 eV, Ts=T1=9 eV and R=.15, with nf=7.5.10e10 fissions, which leads to σ=3.10e3 $(\Omega m)^{-1}$, whereas in the case of Fig.5.7. Tp=50 ev. Ts=T1=7 eV and R=0.02, but at t=50 ns (nf=2.5.10e12).

The results suggest that the increase of neutral density cannot be always considered as a factor that inhibits the growth of ionization rate. Fig. 5.8 shows the stationary values of the relevant parameters as a function of the initial gas density.

Fig. 5.8 shows that the highest values of conductivity are obtained in a region around 10e18 molecules/cm^3. Of course, this value depends on the choice of the input parameters.

Nevertheless, a variation of one order of magnitude of the ionization and recombination coefficients (a and b) slightly affects the results.

The production rate of primary electrons, due to the

fission reactions, plays a relevant role. If an initial rate β of 10e-3 and an initial density of 3.10e18 molecules/cm^3 are assumed, the stationary values become Tp=21 eV, Ts=T1=2.4 eV and R=0.01, i.e. σ =2.10e2 $(\Omega m)^{-1}$ instead of 3.10e3, if the initial value of β is 10e-2.

The distribution of fission rate in the channel is very important in order to maintain suitable conditions for MHD conversion. In fact, if the ionization source stops at a time to (equivalent to a sharp cut in the spatial distribution at xo=Vg.to), the further evolution of the ionization rate R is given by

$$\frac{dR}{dt} = - \frac{bNg^2R^3}{Ts^{7/2}}$$

the secondary electrons being too cold to sustain the ionization level. This equation can be integrated by assuming as initial values those determined, in the stationary state, by the fission source. Thus, the time evolution is represented by $R=Ro/(1+t/\tau)^{1/2}$, where $\tau=Ts^{7/2}/2b(RoNg)^2$.

By introducing the data of Fig. 5.6, R is reduced by a factor 10 in 0.05 μs. It results that in the absence of a ionization source, the conductivity drops quickly to unsuitable values.

The time behavior of temperatures and ionization rate greatly simplifies the analysis of the fuel chemical composition,

with special regard to the formation of negative ions and to the contribution to ionization of the species arising from UF6 dissociation. Dissociation is important from the point of view of the effective neutral density. Reminding the results shown in Fig. 5.8, an increase of neutral density due to dissociation does not affect dramatically the relevant parameters. On the contrary, if the initial density is 5.10e17 molecules/cm^3, as it could be expected during the gas expansion in the MHD channel, a growth of a factor 7, due to dissociation and subsequent ionization, could lead to an improvement of the final degree of ionization and temperatures, whose values should approximate those of Ng=3.5.10e18 molecules/cm^3 (see Fig. 5.8). However, according to the measurements of Compton [7], the thresholds for the formation of UFn+ type ions by electron impact ionization are respectively 14 eV for UF5+, 18 eV for UF4+, 22 eV for UF3+, 26 eV for UF2+, 32 eV for UF+ and 40 eV for U+. Since the stationary temperature of secondary electrons and ions is in the range of 5 eV, relevant contributions can be only expected from UF6 and UF5.

The influence of the formation of negative ions on the conductivity can be estimated by simple arguments. The affinity potential is around 5 eV with a cross section of 3 A^2 [7] (the behavior is similar for UF6- and F-). By averaging over a Maxwell distribution, the contribution of attachment in Eq.(8) can be expressed as

$$\langle \sigma v \rangle n_e (N_F + N_{UF}) = n_e (N_F + N_{UF}) \frac{a_-}{T_s^{1/2}} \exp(-I_-/kT_s) \qquad (cm^3 s)^{-1}$$

where $a_- \approx 10^{-7}$ (cgs units) and $I_- \approx -5$ eV. By introducing this term in Eq.(8), it turns out that the previous results are slightly modified, even in case of total dissociation, i.e. $N_F + N_{UF} = 6N_g$. In particular, the degree of ionization decreases of less than 10% in comparison with the value obtained without attachment.

From the above discussion, it seems that the model of Equations (5)-(8) gives a reliable description of the ionization in conditions of relatively low gas density. The model does not consider inelastic collisions between electrons and neutral atoms, with excitation of internal levels, and transfer of energy between ionized and neutral gas. The influence of these effects can be estimated by comparing the collision frequency with neutrals and between electrons and ions. With the previous notation, the loss of energy by collisions with neutrals can be neglected if (see Eq.(6))

$$\frac{R}{(1-R)} \gg 3.10^{11} Q N T_s^2$$

With QN=10e-15 cm^{-3}, Ts=9 eV, R 2.5.10e-2. The value of R=0.15 (Fig. 5.6) ensures that only about 10 % of energy is tranferred to the neutral gas. As a consequence, the chemical composition of the neutral gas will be simply determined by the thermal equilibrium relations, calculated at the temperature of the neutral gas, being negligible the heating due to ionization. Fig. 5.9 represents the chemical composition of UF6 calculated in conditions of thermal equilibrium at a pressure of 10 atm (from Ref.[8]).

The percentage of neutrals of differents species can be directly obtained from Fig. 5.9 at the temperature of the gas flowing in the channel, whose value is not modified by the ionization processes. Referring for instance to the conditions of Fig. 5.6, the stationary state in the channel can be approximately estimated as:

90% neutral gas, of composition: 95 % UF6, 5 % UF5 (at Tg=2000 K).

10% ionized yields, of composition: 50% UF6+, 50% UF5+, F-<10 % (from the experimental results of Ref.[7])

With an initial density of 3.10e18 molecules/cm^{-3}, we obtain:

2.565.10e18 molecules/cm^{-3} of UF6, 0.135.10e18 molecules/cm^{-3} of UF5, 2.7.10e17 molecules/cm^{-3}, 1.5.10e17 molecules/cm^{-3} of UF6+ and UF5+, less than 3.10e16 molecules/cm^{-3} of F-.

Finally, Figures 5.10-5.12 report the results obtained with the gas density distribution of Fig. 5.3, and the fission density distribution of Tab. 5.1. The latter is conservative: the

preliminary evaluation of the influence of wall material and thickness reported in Tab. 5.2 shows the potential for the fission and gamma densities in the duct to be increased of one order of magnitude at least, in comparison with the values used for the conductivity calculations, if a material with favourable nuclear properties is adopted.

11 References

[1] Rosa R.J., "Magnetohydrodynamic Energy Conversion", Revised Printing, Hemisphere Publishing Corporation, 1987.

[2] Rockwell III T., "Reactor Shielding Design Manual", First Edition, D. Van Nostrand, Princeton.

[3] Daneri A., Gabutti B., Salina E. "SOUID-360 - A Multigroup Diffusion Program with Criticality Searches for the IBM-360", EUR 3881e 1968.

[4] Devillers C. and Dubont C., "Mercure-IV, un programme de Monte Carlo a trois dimensions pour l integration de novaux ponctuel d attenuation en ligne droite", Report SERMA - T - 496 1980.

[5] Devillers C. and Dubont C., "Creation de la Bibliotheque Multigroupe Gamma BIP/G2", 1973.

[6] for an extended description of the phenomena under study, see:
L. Spitzer, "Physics of Fully Ionized Gases", Interscience, New York 1956;

Zeldovich and Raizer, "Physics of Shock Waves and High-Temperature Hydrodynamic Phenomena", Academic Press, New York 1966;

V.L. Gilzburg, "The Propagation of Electromagnetic Waves in Plasmas", Pergamon Press, 1964.

[7] Comoton R.N., "On the Formation of Positive and Negative Ions in Gaseous UF6", J. of Chem. Phys., Vol 66 No 10, 1977.

[8] Kazanskii K.A. and Novikov V.M., "Thermophysical and Electrophysical Properties of Uranium Hexafluoride at Temperatures of (1-11)·10³ K and Pressures of 0.1-100 atm", Translated from Teplofizika Vysokikh Temperatur, Vol. 14 No 3, Plenum Publishing Corporation, New York 1976.

Tab. 5.1 Fission power density in the MHD channel, simplified calculations.

Distance from Entrance of Nozzle (cm)	Fission Power Density (MeV / cm3 sec)
50	1.72 E+12
200	2.90 E+10
400	2.80 E+09
600	9.20 E+08

Tab. 5.2 Fission power density in the MHD channel, diffusion calculations (MeV/cm3 s).

REGIONS	Al2O3 Thickness a 3 cm Aver.Power Density	Ratio a/a	b 6 cm Aver.Power Density	Ratio b/a	BeO Thickness c 3 cm Aver.Power Density	Ratio c/a	d 6 cm Aver.Power Density	Ratio d/a
1	1.10E+14	1.0	1.35E+14	1.22	2.10E+14	1.9	3.20E+14	2.9
2	6.54E+12	1.0	9.61E+12	1.47	2.10E+13	3.2	4.70E+13	7.2
3	9.45E+11	1.0	1.85E+12	1.96	3.00E+12	3.2	1.20E+13	12.76
4	1.93E+11	1.0	4.62E+11	2.4	7.51e+11	3.9	4.08E+12	21.2
5	4.42E+10	1.0	1.23E+11	2.78	2.08E+11	4.7	1.40E+12	31.7
6	7.99E+09	1.0	2.56E+10	3.2	4.95E+10	6.2	4.08E+11	51.1
7	4.25E+08	1.0	1.70E+09	4.0	3.91E+09	9.2	4.19E+10	98.6
8	1.83E+08	1.0	8.22E+08	4.5	1.96E+09	10.7	2.36E+10	129.2
9	1.37E+08	1.0	6.55E+08	4.8	1.58E+09	11.6	1.96E+10	143.3

Tab. 5.3 Gamma power density in the MHD channel.

Distance from Entrance of Nozzle (cm)	Gamma Power Density (MeV / cm3 sec)
0	2.72 E+11
100	4.81 E+09
200	4.39 E+08
300	1.72 E+08
400	8.45 E+07
500	4.98 E+07
600	1.03 E+07
700	7.33 E+06
800	5.39 E+06
900	4.00 E+06
1000	3.14 E+06
1100	2.50 E+06
1200	2.07 E+06

1		10	Al2O3
2		11	Graphite
3		12	BeO
4		13	Zr/Nb Alloy
5	UF6	14	Be
6			
7			
8			
9			

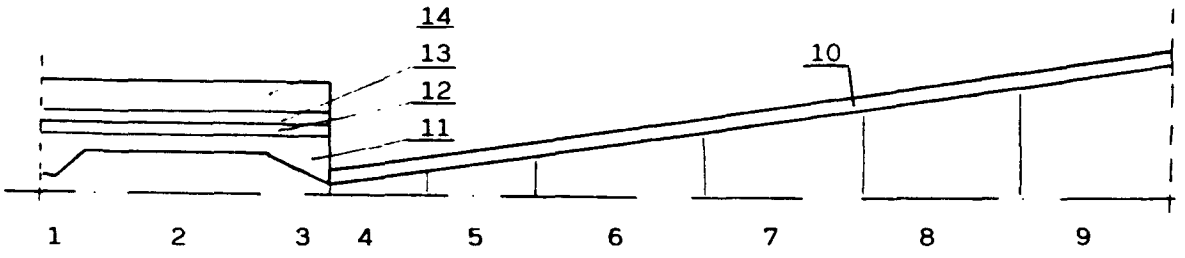

Fig. 5.1 Three dimensional model for fission density simplified calculations and Mercure calculations.

1		11	TZM
2		12	Graphite
3		13	BeO
4		14	Zr/Nb Alloy
5	UF6 Nozzle and MHD Channel	15	Be
6		16	Al203 or BeO
7			
8			
9			
10	UF6 Core		

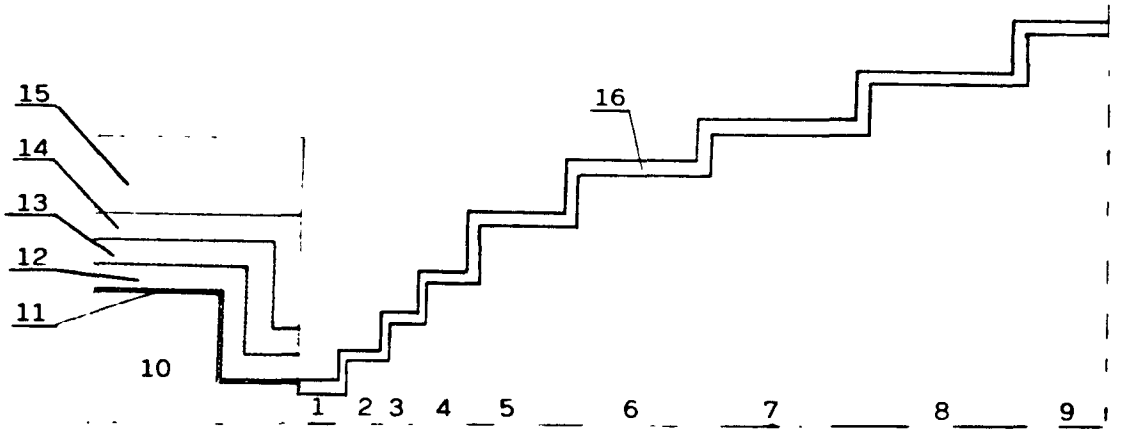

Fig. 5.2 Two dimensional model for SQUID calculations.

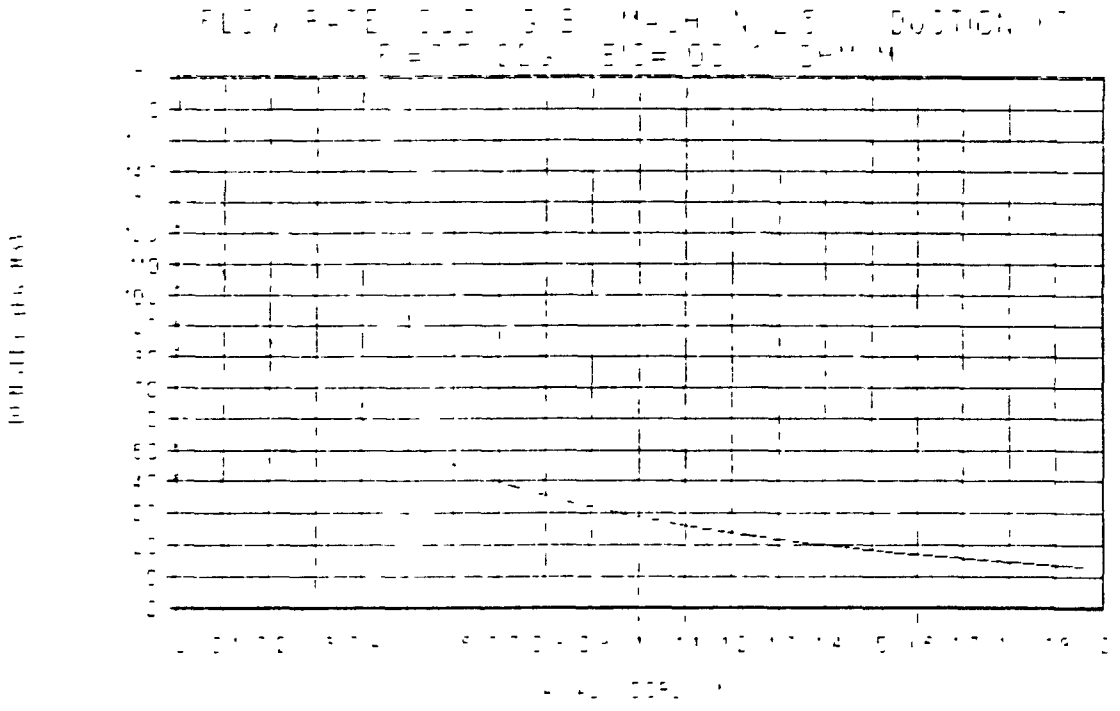

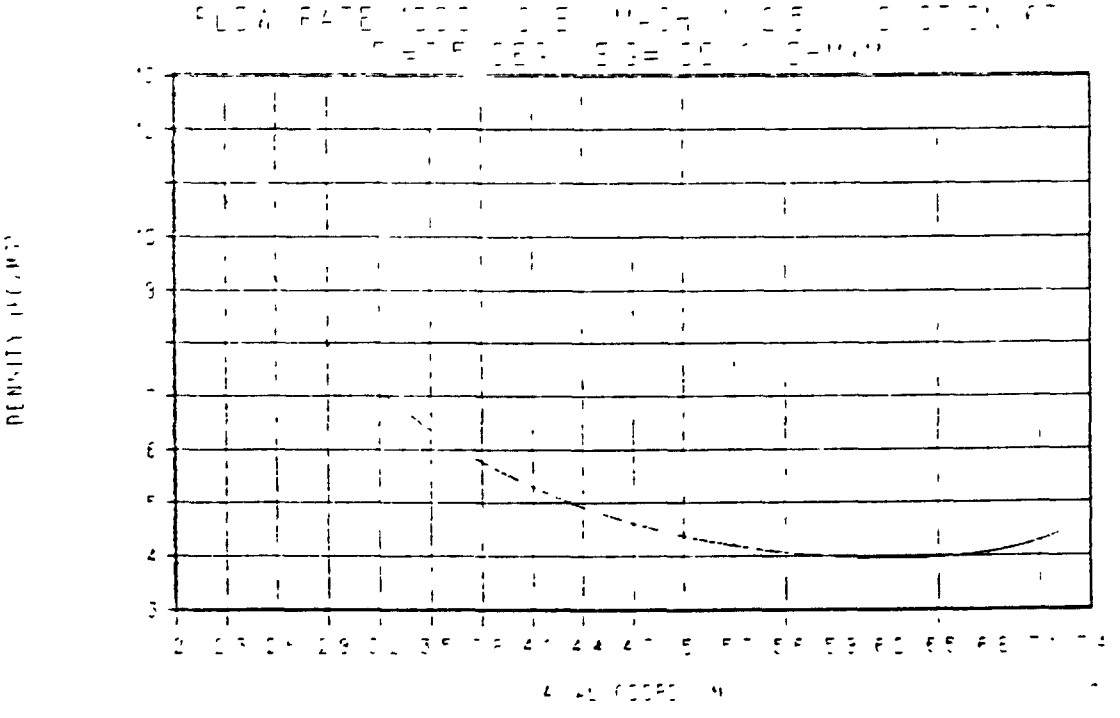

Fig. 5.3 UF6 density vs. axial coord. in nozzle and channel.

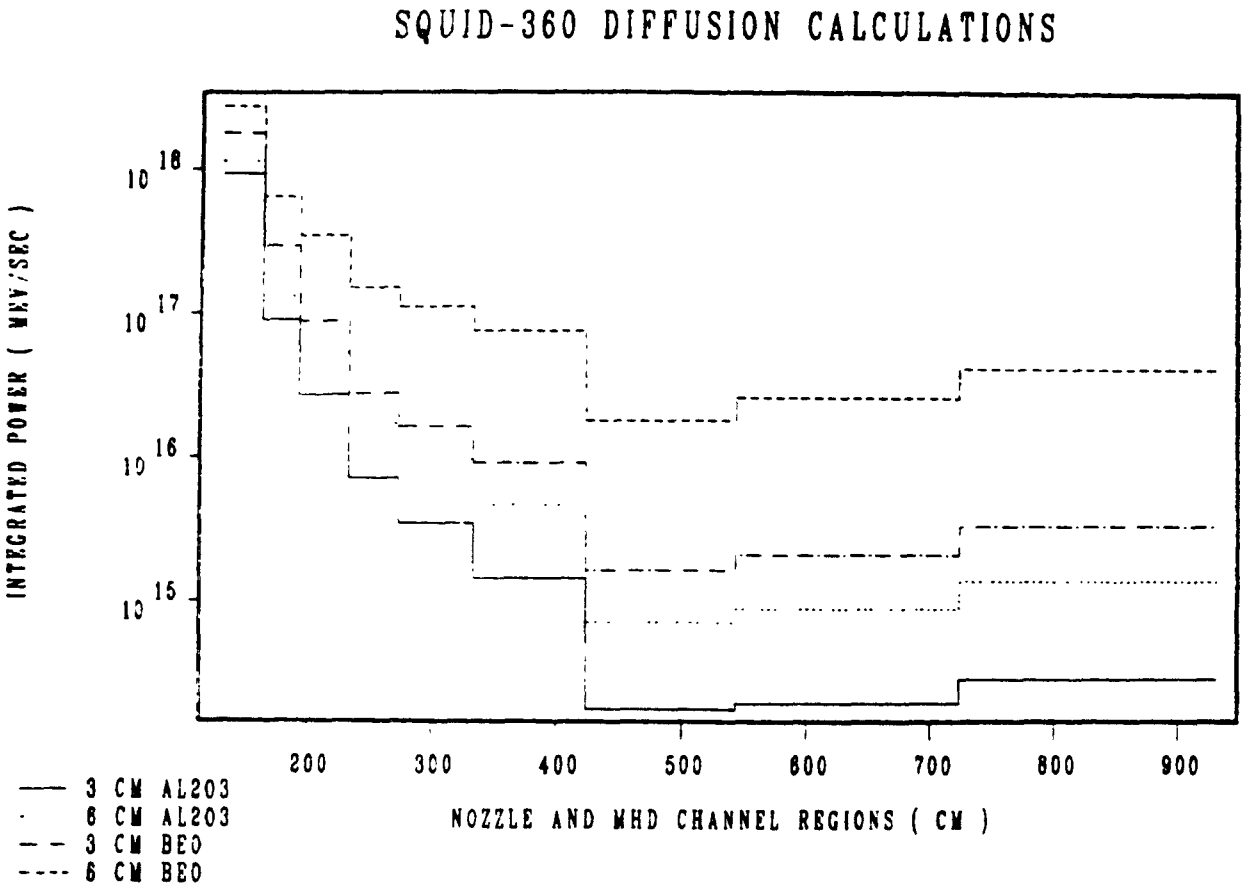

Fig. 5.4 Integrated power for each region.

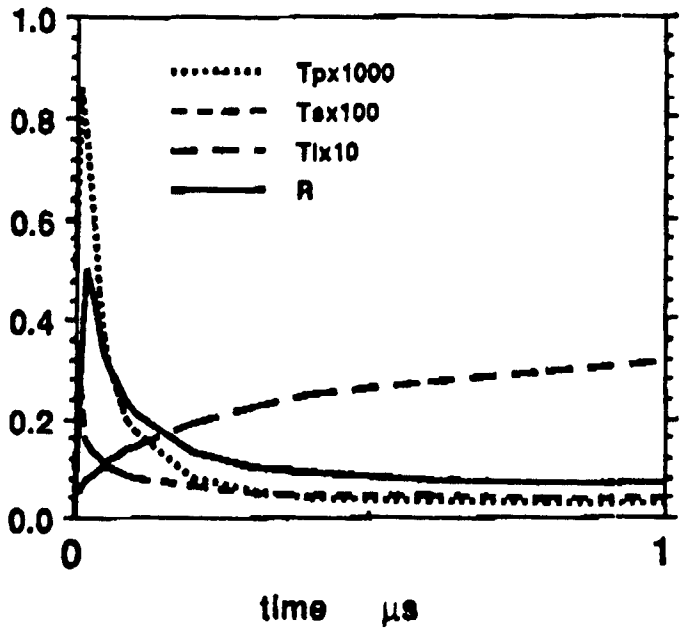

Fig. 5.5 Gas density 5.10e17 molecules/cm3.
Temperatures in eV. nf=1.25.10e10
fissions/s.

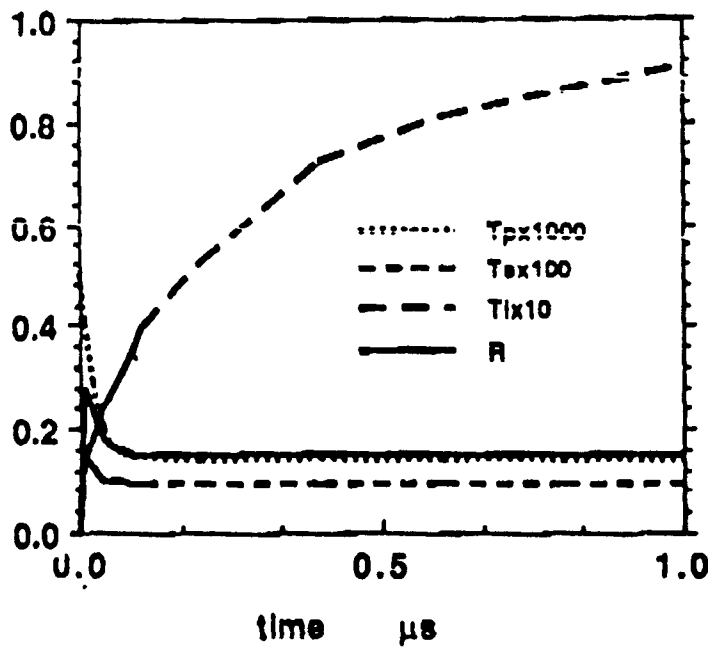

Fig. 5.6 Gas density 3.10e18 molecules/cm3.
Other conditions as in Fig. 5.5.

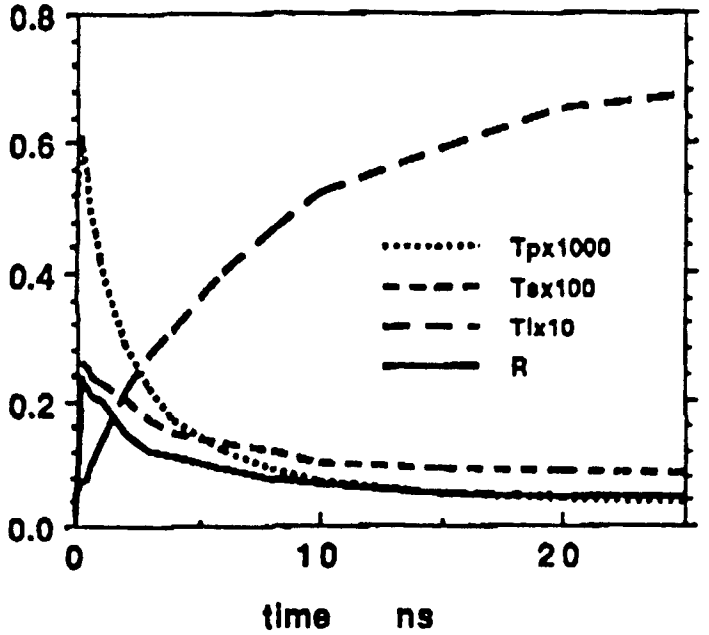

Fig. 5.7 Gas density 10e20 molecules/cm3.
Note the ns scale.

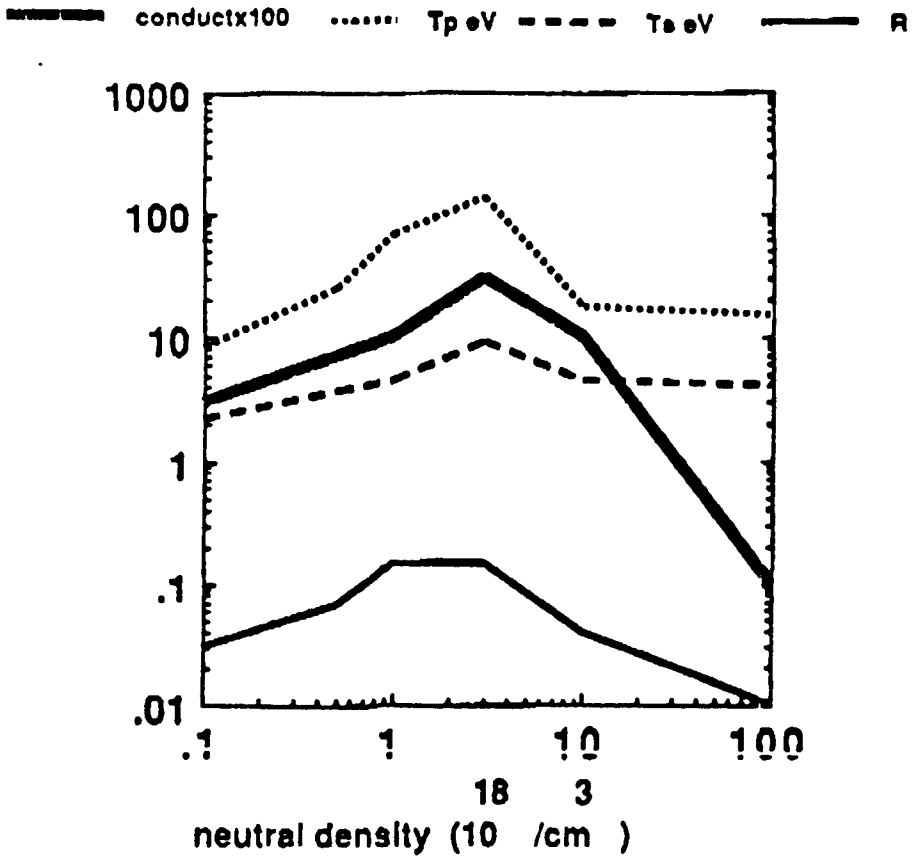

Fig. 5.8 Stationary values of Tp, Ts=Ti, R, and vs. gas density.

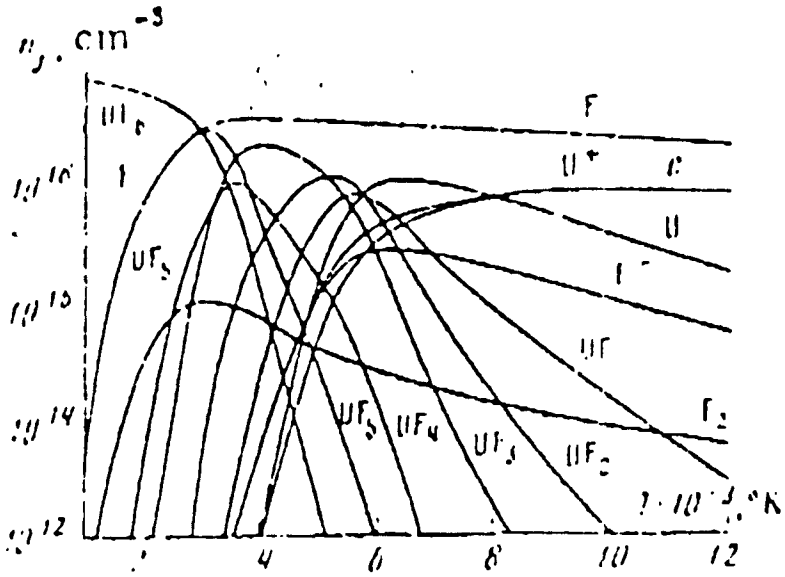

Fig. 5.9 Equilibrium chemical composition of UF6 at 10 atm. (from Ref.8).

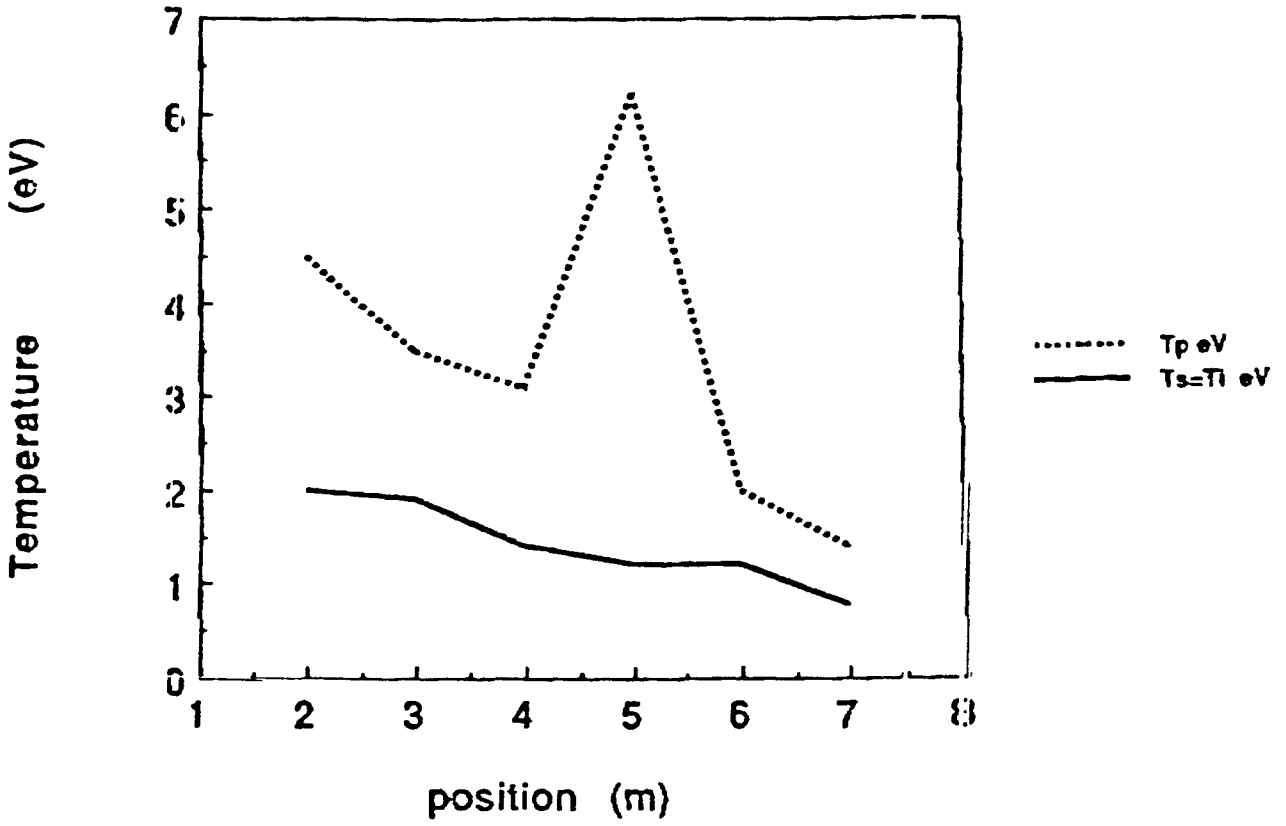

Fig. 5.10 Stationary temperatures vs. position.

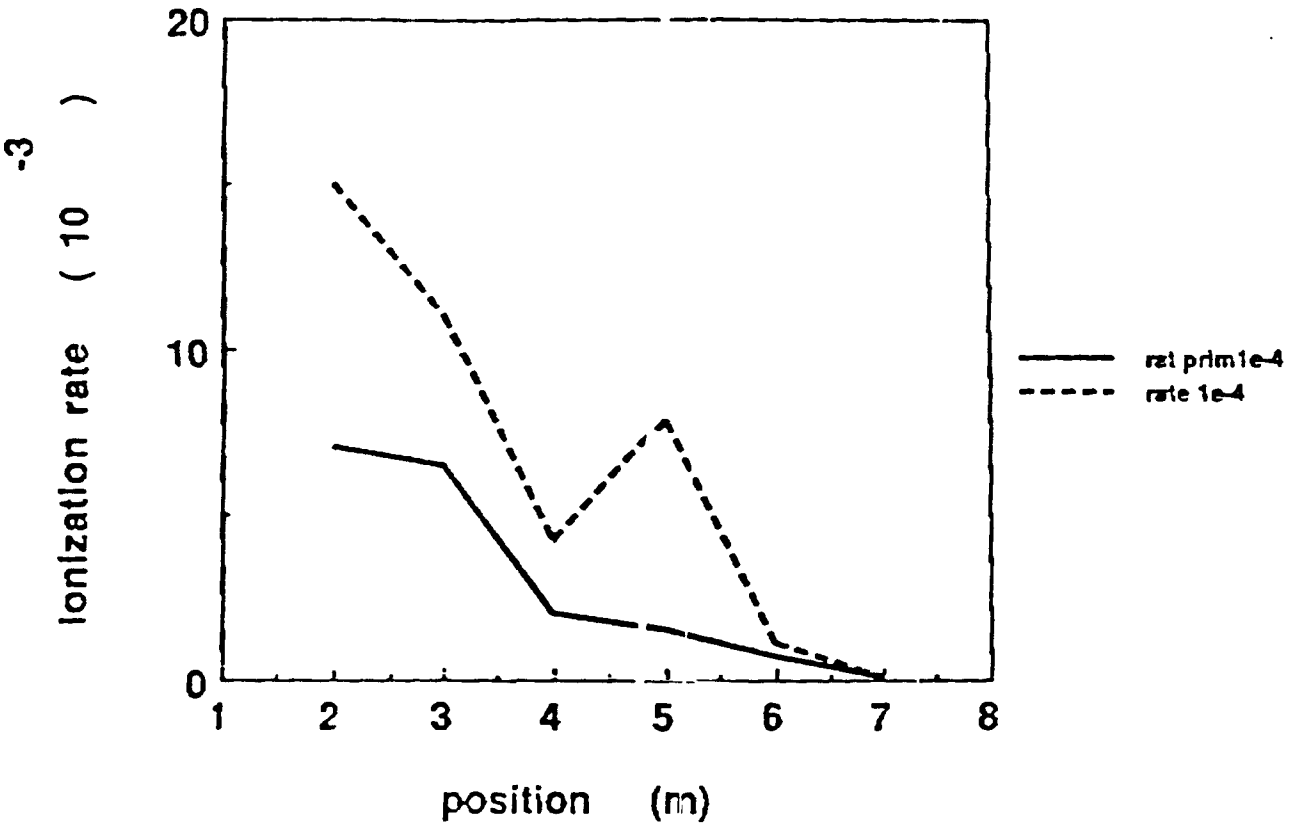

Fig. 5.11 Stationary ionization rates vs. position.

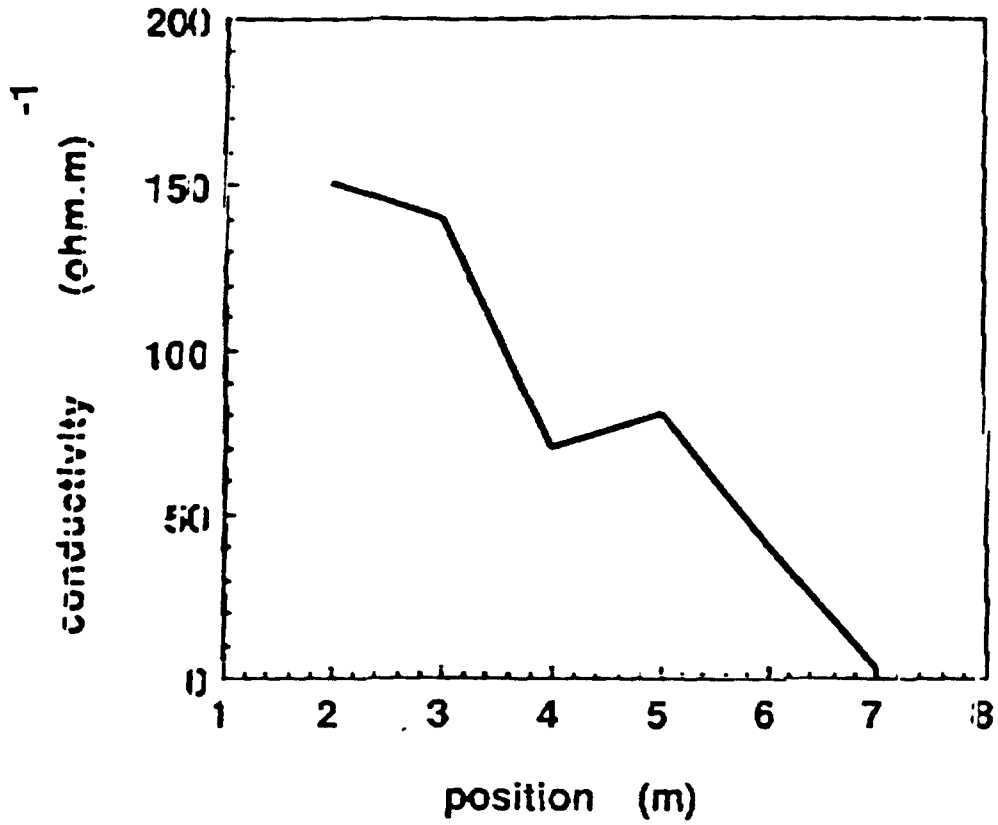

Fig. 5.12 Stationary conductivity vs. position.

6 SUMMARY AND CONCLUSIONS

This report presents the results of work performed under DOE contract number DE-AC22-88PC88651. The overall objective of this project was to investigate the use of a gas-core nuclear reactor directly coupled to an MHD expansion channel in an SDIO mission application. In the proposed concept, working gas could be either uranium hexafluoride or a mixture of uranium hexafluoride and helium, while reactor control is performed by changing the configuration of a reflector located outside the pressure vessel. Work was focused on the basic physical mechanisms of neutronics, reactivity control, ionization, and electrical conductivity of the concept. Specific goals of the project were:

- To evaluate the performance of the external reflector.
- To determine the influence of additional, fission-induced mechanisms on the ionization levels of the working fluid.
- To estimate the electrical conductivity levels that can be attained in the MHD channel, taking into account the effects of F- or other negative ions.

Task 1., Reflector Modeling, provided a reactor configuration that was used as a reference for subsequent, detailed simulation. This configuration is featured by a cylindrical reactor cavity, surrounded by a couple of reflecting (and refractory) shells located inside the pressure vessel and by a movable sliding reflector, located outside the pressure vessel. Two conical

segments, at each end of the cylindrical core, complete the reactor. A simple axial-inlet flow pattern has been adopted in the analysis.

A number of important features of the proposed gaseous reactor were investigated. The nuclear analysis addressed the following items:

a) materials selection for the fixed reflectors inside the reactor pressure vessel, and for the movable reflector;

b) reactivity control performance of the movable reflector;

c) power density distributions inside the core accounting for the interaction with local fuel density and temperature, as resulting from thermal-fluid analysis.

d) reactivity requirements.

Task 2., Working Fluid Characteristics, addressed the study of the ionization levels in the working gas, identifying a mechanism to convert the energy released by the fission reactions into charged particles, and providing a system of rate equations for the numerical estimates performed in Task 3..

Task 3., Electrical Conductivity Effects, provided the evaluation of the conductivity levels attainable in the generator.

To enable this evaluation, the nuclear analysis was extended to include the estimate of fission and gamma power densities inside the nozzle and the MHD channel, taking into account the effects of the wall material and thickness. The rate equations were solved for a number of typical gas conditions and duct

lengths. The influence of dissociation and ion attachment, not included in the simplified numerical approach, was also discussed.

Two major conclusions can be drawn from the accomplishment of this project:

- A reactor configuration has been obtained which avoids to decouple the neutronics of the cavity and its internal reflector from the external shell, thus enabling the latter to be used for reactivity control.

In particular, the results show that the movable reflector is able to make the reactor subcritical by 1000 pcm at least, to control the reactor from CZP to HFP condition, accounting for a reactivity change up to 3300 pcm associated to depletion.

- The conditions expected in the MHD channel show that the ionization and conductivity levels can be amplified through 'secondary' processes induced by the 'primary' hot electrons which are directly generated in the fission reactions.

The numerical calculations suggest that conductivity levels in the range 10-100 $(\Omega m)^{-1}$ are consistent with the characteristics of short nozzle, high power density generators. In fact, the nozzle length turns out to be of critical importance because of the sharp decrease of residual fission and gamma densities as a function of the distance from the reactor outlet.

This conclusion remains true even if the effects of dissociation and attachment are included in the numerical model.

Furthermore, a preliminary evaluation of the influence of wall material and thickness shows the potential for the fission and gamma densities in the duct to be increased of one order of magnitude at least, in comparison with the values used for the conductivity calculations, if a material with favourable nuclear properties is adopted.

7 REPORT DISTRIBUTION LIST

ADDRESS	NUMBER OF COPIES
Mr. Leo E. Marovsky Project Manager U.S. Department of Energy Pittsburgh Energy Technology Center P.O. Box 10940, M.S. 922-206 Pittsburgh, PA 15236	2
Ms. D. J. Tamilia U.S. Department of Energy Pittsburgh Energy Technology Center P.O. Box 10940, M.S. 922-206 Pittsburgh, PA 15236	2
Mr. Gary E. Staats U.S. Department of Energy Pittsburgh Energy Technology Center P.O. Box 10940, M.S. 922-206 Pittsburgh, PA 15236	1
Keith R. Miles Contract Specialist U.S. Department of Energy	1

Pittsburgh Energy Technology Center

P.O. Box 10940, M.S. 900-33

Pittsburgh, PA 15236

U.S. Department of Energy 3

Pittsburgh Energy Technology Center

Office of Technology Transfer

P.O. Box 10940, M.S. 922

Pittsburgh, PA 15236

Mr. Jorgen Birkeland 1

U.S. Department of Energy

FE-15, C-121/GTN

Washington, DC 20545

Chicago Operations Office 1

General Counsel for Patents

9800 South Cass Avenue

Argonne, IL 60439

Mr. Richard Verga 1

SDIO/SLKT

Pentagon

1717 H. Street

Room 748

Washington, DC 20301-7100

Mr. George Rudins 1

U.S. Department of Energy

FE-32, D-107/GTN

Washington, DC 20545